



저작자표시-비영리-변경금지 2.0 대한민국

이용자는 아래의 조건을 따르는 경우에 한하여 자유롭게

- 이 저작물을 복제, 배포, 전송, 전시, 공연 및 방송할 수 있습니다.

다음과 같은 조건을 따라야 합니다:



저작자표시. 귀하는 원저작자를 표시하여야 합니다.



비영리. 귀하는 이 저작물을 영리 목적으로 이용할 수 없습니다.



변경금지. 귀하는 이 저작물을 개작, 변형 또는 가공할 수 없습니다.

- 귀하는, 이 저작물의 재이용이나 배포의 경우, 이 저작물에 적용된 이용허락조건을 명확하게 나타내어야 합니다.
- 저작권자로부터 별도의 허가를 받으면 이러한 조건들은 적용되지 않습니다.

저작권법에 따른 이용자의 권리는 위의 내용에 의하여 영향을 받지 않습니다.

이것은 [이용허락규약\(Legal Code\)](#)을 이해하기 쉽게 요약한 것입니다.

[Disclaimer](#)

Master's Thesis
석사 학위논문

Flexible and Stretchable Strain Sensor for Monitoring of Bladder Volume

Yujin Jo(조 유 진 趙洵璿)

Department of
Robotics Engineering

DGIST

2021

Flexible and Stretchable Strain Sensor for Monitoring of Bladder Volume

Advisor: Professor Sanghoon Lee
Co-advisor: Professor Hoejoon Kim

by

Yujin Jo
Department of Robotics Engineering
DGIST

A thesis submitted to the faculty of DGIST in partial fulfillment of the requirements for the degree of Master of Science in the Department of Robotics Engineering. The study was conducted in accordance with Code of Research Ethics¹

12. 29. 2020

Approved by

Professor Sanghoon Lee (signature)
(Advisor)

Professor Hoejoon Kim (signature)
(Co-Advisor)

¹ Declaration of Ethical Conduct in Research: I, as a graduate student of DGIST, hereby declare that I have not committed any acts that may damage the credibility of my research. These include, but are not limited to: falsification, thesis written by someone else, distortion of research findings or plagiarism. I affirm that my thesis contains honest conclusions based on my own careful research under the guidance of my thesis advisor.

Flexible and Stretchable Strain Sensor for Monitoring of Bladder Volume

Yujin Jo

Accepted in partial fulfillment of the requirements for the degree of Master of
Science.

11. 30. 2020

Head of Committee Prof. Sanghoon Lee (signature)

Committee Member Prof. Hoejoon Kim (signature)

Committee Member Prof. Hongki Kang (signature)

ABSTRACT

One of emerging issues in aging society is a bladder dysfunction which refers urinary bladder problems due to disease or injury. Nowadays, many people around the world have been suffered from it and the number of the patient is continuously increasing now. It makes the patient's daily life difficult and isolate them. Currently, clinical approaches are valid, but there are many limitations. Accordingly, many researchers in various fields such as biomedical engineering and neural engineering conducted novel methods to treat bladder dysfunction. Recently, it has been reported that one of promising solutions for treating the bladder dysfunction, especially for underactive bladder (UAB) is a neuromodulation method where a neurostimulator is implanted into the body and delivers currents to bladder nerves to induce the micturition. For this approach, neural interfaces and neurostimulators for UAB are required. Furthermore, an effective method for monitoring of bladder status is required for applying the treatment using the neurostimulation in a timely manner. For this, there were previous studies of bladder sensors including implantable or non-invasive approaches, however, these have limitations in terms of sensitivity, correlation between pressure and sensor output, and inconsistency of materials characteristics.

This paper demonstrates highly flexible and stretchable strain sensors fabricated with biocompatible materials for bladder monitoring applications. The bladder is a high-stretchable organ, so the length of its wall is stretched by up to 3 times. To match the characteristics of the bladder, Ecoflex, which has biocompatible, high-stretchable, and a low Young's modulus (~83 kPa) characteristics, is used as a substrate material of the sensor. Also, carbon nanotube (CNT), well-known as a highly conductive material, is used as a conducting material of the strain sensor for the simplicity of the fabrication as well as for the stretchable characteristics on the substrate. A spray coating method is used to form a CNT thin film on the substrate, and AuCNT composites are additionally deposited on the CNT thin film by an electrodeposition method to improve the low sensitivity of the CNT strain sensors. First, the sensors with CNT and AuCNT composites are designed in a simple stick shape to compare the performance of the device. The resistance characteristics of each strain sensor depending on the strain change within 200 % are measured. The results indicate that the strain sensors with AuCNT composites are more sensitive than the one with CNT.

Furthermore, a 3-channel strain sensor is developed to track the movement of bladder wall. The 3-channel strain sensor with AuCNT composites is fabricated to cover a bladder. In addition, a monitoring system is also developed using Arduino to track the resistance change of the sensors according to water flow. After that, the performance of 3-channel strain sensor is demonstrated with a balloon model as well as an *ex-vivo* bladder of

pigs using this system. The overall results show that the sensors with the monitoring system could be applicable for bladder applications with an implantable neurostimulator, providing a closed-loop neuromodulation.

Keywords: Strain sensor, Bladder dysfunction, Bladder monitoring system, Closed-loop neuromodulation

List of Contents

Abstract	i
List of contents	ii
List of tables	iii
List of figures	vi
I. Introduction	1
II. Experimental Methods	6
2.1 Fabrication	6
2.2 Strain-Resistance Measurement	11
2.3 Volume-Resistance Measurement	13
2.4 Balloon-Model Test	15
2.5 Volume Monitoring	15
2.6 <i>Ex-vivo</i> Test with Pig's Bladder	15
2.7 3-Channel Strain Sensor	16
III. Results and Discussion	18
3.1 Fabrication Conditions of CNT Strain Sensor	18
3.2 Comparison of CNT and AuCNT Strain Sensor	22
3.3 Balloon-Model Monitoring	26
3.4 <i>Ex-vivo</i> Test with Pig's Bladder	29
3.5 3-Channel Strain Sensor	32
IV. Conclusion	41
References	42

List of Tables

Table 1. Previous bladder sensors.	4
Table 2. Young's modulus and stretchability of bladder and biocompatible substrate materials.	4

List of Figures

Figure 1. Bladder dysfunction patient and closed-loop system for treating of bladder dysfunction.	1
Figure 2. Previous studies of bladder monitoring sensors and methods.	3
Figure 3. Fabrication process of strain sensors.	7
Figure 4. Electrodeposition of AuCNT composites.	9
Figure 5. AuCNT strain sensor.	10
Figure 6. Strain-Resistance measurement.	12
Figure 7. Volume-Resistance measurement platform with Arduino.	14
Figure 8. 3-channel strain sensor.	17
Figure 9. Comparison of characteristics of the CNT strain sensor by curing temperature between 50 °C and 70 °C.	20
Figure 10. Comparison of characteristics of the CNT strain sensor by amount of CNT water dispersion.	21
Figure 11. The comparison result of the CNT strain sensors and AuCNT strain sensors. ..	23
Figure 12. Cross-section SEM images of the CNT strain sensor.	24
Figure 13. Cross-section SEM images of the AuCNT strain sensor.	25
Figure 14. Volume-Resistance measurement in Balloon-Model.	27
Figure 15. Volume monitoring with Arduino system.	28
Figure 16. <i>Ex-vivo</i> test with pig's bladder.	30
Figure 17. Volume-Resistance characteristics with pig's bladder.	31
Figure 18. The fabricated 3-channel strain sensor.	32
Figure 19. Volume-Resistance characteristics with the 3-channel strain sensor on a balloon-model.	33
Figure 20. Expansion detecting of the balloon-model.	35

Figure 21. The 3-channel strain sensor sutured on the bladder wall. 36

Figure 22. Volume-Resistance characteristics of 3-channel strain sensor with a pig's bladder.
..... 37

Figure 23. *Ex-vivo* test of 3-channel strain sensor for detecting of expansion directions. .. 38

Figure 24. Bladder expansion according to the volume. 39

I. INTRODUCTION

Bladder dysfunction is one of emerging issues in aging society that threatens normal daily life [1]. Hundreds of millions of people around the world have been suffered from it, and the number of the patient is continuously increasing now [2]. Most of bladder dysfunction are relevant to the damage of neural function, called neurogenic bladder, which involves urinary problems unable to control of urination [1]. Several factors cause the neurogenic bladder such as diseases and injuries [1]. For instance, the patients who get spinal cord injury suffers the bladder dysfunction temporarily or permanently, which make the patient difficult to spend normal life [1]. Another problem of the bladder dysfunction is that it causes other diseases unless urination occurs in a timely manner. Accordingly, some practical solutions are suggested in hospitals, but those are still challenge in returning the patients to normal life. Medical doctor, biomedical engineer, and neural engineers are struggling to address the bladder dysfunction, and biomedical companies shows interest in this issue. One of promising solution, especially for underactive bladder (UAB), is to implant a neurostimulator into the body, and to stimulate relevant to bladder nerves to induce micturition, which showed promising results. [1, 3]. However, due to the damage of the sensory neurons in the bladder, the patient is not able to sense the moment when bladder is full. Therefore, in order to apply the treatment using the neurostimulation in a timely manner, a monitoring system that measure bladder status is required.

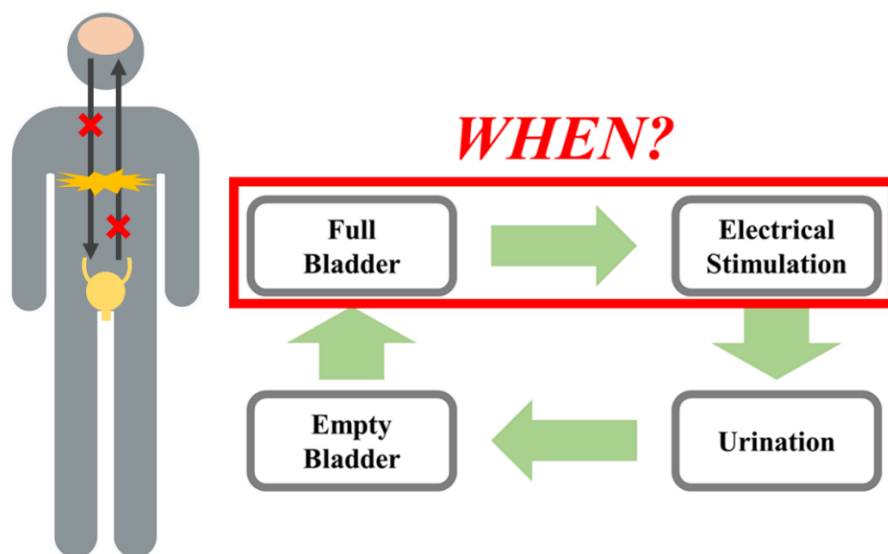


Figure 1. Bladder dysfunction patient and closed-loop system for treating of bladder dysfunction.

To develop a bladder sensor to properly monitor bladder changes, we first need to know the interesting characteristics of the bladder. The bladder is a stretchable saclike organ that stretches its length by up to 3 times when full of urine [4, 5]. Also, the bladder's muscle wall contracts for the urination, becoming thicker and firm when empty. Furthermore, the bladder is a soft organ, known to have a low Young's modulus. Elastic modulus of bladder is known, rat's bladder is 0.76 MPa and pig's or human's bladder is 0.25~0.26 MPa [6]. Especially, the pig's bladder is known to have nearly the same characteristics as a human bladder, applying it highly suitable for research to treat the patients with bladder dysfunction.

There are typically two ways to measure bladder pressure. The first one is to implant a sensor inside the bladder or the bladder wall to measure intra-pressure of the bladder. However, due to severe environment inside the bladder such as the presence of urine and dramatical pressure change, the packaging of the sensor to endure the chemical and the physical change is one of challenging issues. Recording the reliable pressure by such sensor in the environment and the transmission of the output signal outside the body are also critical issues. The second one is to attach a sensor on the surface of bladder wall to measure the volume change of the bladder. For instance, a stick-shaped sensor attached to the bladder wall stretches together with the expanding bladder, providing the volume change of the bladder through the output change of the sensor. However, the bladder is a 3-D object, the rate of change of the sensor are different depending on the direction in which the sensor is attached [2]. Therefore, a small size of the stick-shaped sensor is not enough and does not accurate to measure overall bladder volume changes.

There were many studies of sensors that monitor the volume of the bladder, and there were different types of sensors according to the operating mechanisms. Figure 2 and Table 1 show various prior studies according to sensing methods. The bladder sensors were studied with many sensing methods, including (a) resistive [2, 7, 8, 9], (b) capacitive sensors [7, 10], (c) accelerometer [11], (d) piezoelectricity [12], piezoresistive sensors [13], and (e) triboelectric nanogenerators (TENGs) [14]. However, each of these methods has its own drawbacks. First, capacitive-type sensors are difficult to apply to a circuit since the output value is small depending on the strain [7]. Also, one capacitive-type sensor showed limited sensing volume ranges (100~200 ml) and operation frequency ranges (8.5~9.5 MHz) [10]. And the study where an accelerometer and a piezoelectric sensor were implanted inside the bladder wall is likely to damage the bladder wall muscle and limited clinical applications [11, 13]. In addition, the method using TENGs requires special equipment to measure the output signal like an

oscilloscope due to the high internal impedance of the device, as well as the enough output signal is only generated during the large mechanical movements of the target. Due to the unique characteristics of the bladder, resistive-type sensors are appropriate for the volume monitoring of the bladder. It has a simple mechanism and is relatively easy to apply to a circuit. Actually, there was more research on resistive type sensors than the other types of sensors for the bladder applications as shown in Table 1. However, the improvement of sensor performance in terms of volume, length, sensitivity with a proper monitoring system is still required for the bladder applications.

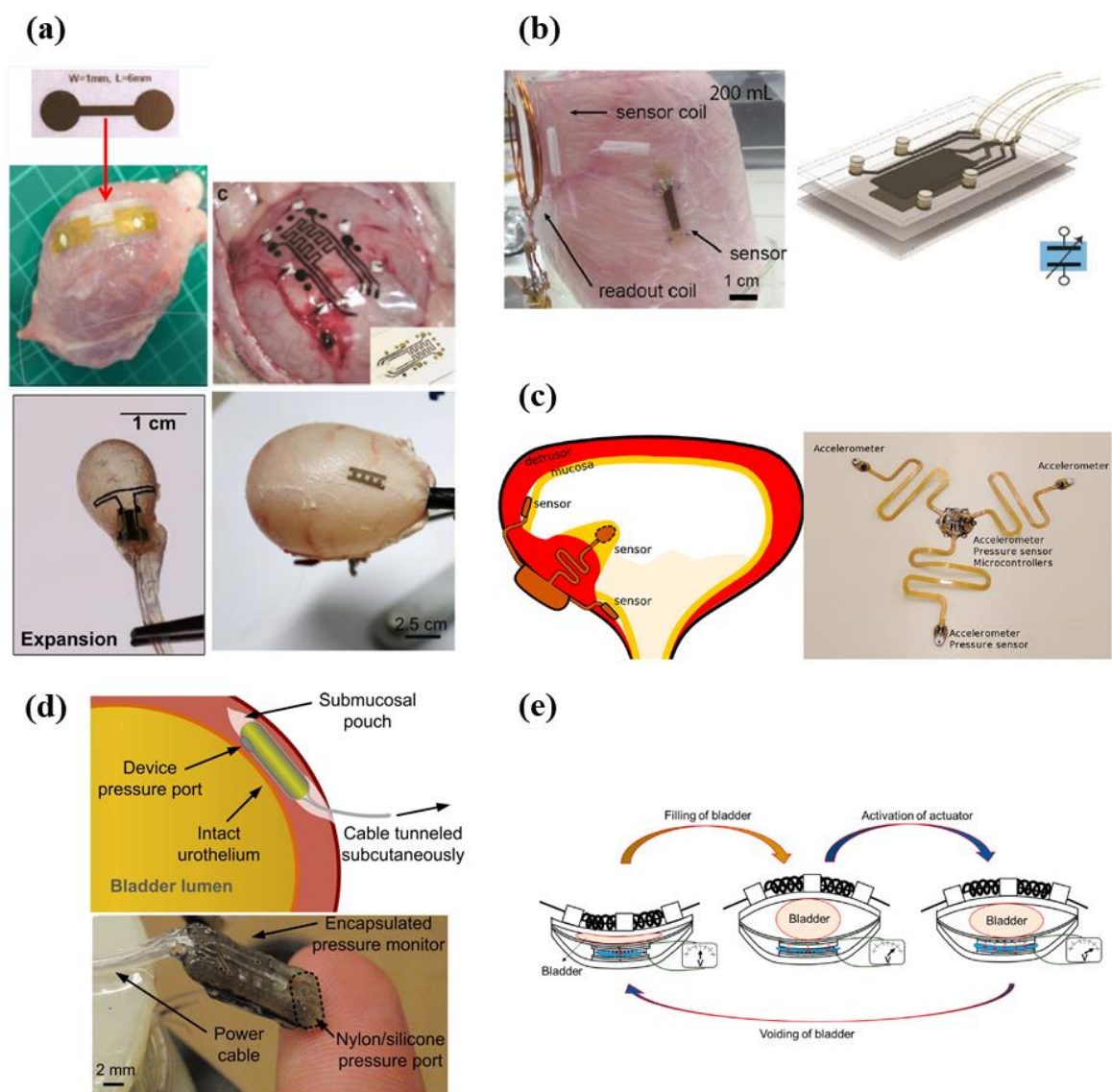


Figure 2. Previous studies of bladder monitoring sensors and methods. (a) Resistive type. (b) Capacitive type. (c) Accelerometer. (d) Piezoelectricity. (e) TENG.

<i>Reference</i>	<i>Sensor type</i>	<i>Materials</i>	<i>Target bladder</i>	<i>Sensing range</i>	<i>Output range</i>
[2]	Resistive	Cr/Au – PU	Pig	60 ~ 140 mL	16 ~ 24 Ω
[7]	Resistive	SWCNT – Ecoflex 0050	Feline	0 ~ 50 mL	~ 3.7 (R/R_0)
[8]	Resistive	CB – Ecoflex 0030	Rat	3.2 ~ 18.4 mmHg	0.3 ~ 0.4 M Ω
[9]	Resistive	Polypyrrole / Agarose Hydrogel	Pig	~ 658 mL	-
[7]	Capacitive	SWCNT – Ecoflex 0050	-	~ 100 % strain	160 ~ 375 pF
[10]	Capacitive (LC Resonance)	Au-TiO ₂ NW - PDMS	Pig	100 ~ 200 mL	8.5 ~ 9.5 MHz

Table 1. Previous bladder sensors.

In order to develop resistive-type strain sensors for the monitoring of bladder volume, it is important to select materials that match the characteristics of the bladder mentioned above. Table 2 compares Young’s modulus and the stretchability of bladders with the materials used in previous studies. When two materials with different Young’s modulus are attached in parallel, total Young’s modulus is the sum of modulus of these two materials. Therefore, materials with low Young’s modulus should be used to make the bladder encounter less stress as the bladder expands. In addition, materials with high stretchability (200~ % strain) should be used to extend with the bladder wall as it expands.

<i>Materials</i>	<i>Young’s modulus (kPa)</i>	<i>Stretchability (%)</i>
Rat bladder	760 [6]	-
Pig bladder	260 [6]	200 [5]
Human bladder	250 [6]	-
PDMS	1840 [15]	130 [16]
Ecoflex 0050	83 [15]	980*
Ecoflex 0030	69 [15]	900*
TPU	3340 [17]	331 [17]

* by Smooth-On, Inc.

Table 2. Young’s modulus and stretchability of bladder and biocompatible substrate materials.

According to Table 2, among the materials mainly used in flexible and stretchable biological electrodes, PDMS has too low stretchability to be applied to bladder. And the thermoplastic polyurethane (TPU) has more than 300 % strain stretchability, but Young’s modulus is too high for the bladder. Therefore, Ecoflex is appropriate as a substrate material for bladder monitoring strain sensors, which has more than 900 % strain stretchability and Young’s modulus of one-third that of pig’s bladder.

Stretchable conductive material is also required to reliably maintain electrical conductivity when a sensor is

stretched. There are many conductive materials being used in strain sensor. Among them, carbon nanotube (CNT) has proven to be capable of up to 500 % strain, used with Ecoflex [18]. Also, there are various options for the fabrication of CNT thin film, including spray coating [18, 19], spin coating [20], chemical vapor deposition (CVD) growth [21], stamping [22, 23], inkjet printing [24]. Among them, the spray coating method is selected for this paper since it is simple and low-cost.

In this study, we developed flexible and stretchable strain sensors using Ecoflex and CNT to measure the volume of the bladder. And, to enhance the performance of the device, we additionally coated AuCNT composites on the CNT thin film. The resistance characteristics of the proposed strain sensors depending on the strain change within 200 % were measured. Furthermore, to track the expansion direction of a bladder, a 3-channel strain sensor was developed. The 3-channel strain sensor with AuCNT composites was fabricated to cover a bladder.

In addition, a monitoring system was also developed using Arduino to track the resistance change of the sensors according to water flow. The performance of the sensors was demonstrated with a balloon-model and pig's bladders using the developed monitoring system.

II. EXPERIMENTAL METHODS

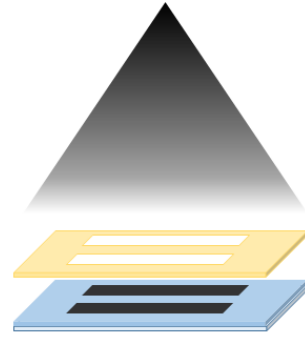
2.1 Fabrication

Figure 3 shows the overall fabrication process of a strain sensor. The fabrication process of the strain sensor started from a spin coating of photoresist (AZ9260, AZ Electronic Materials Ltd.) to be used as a sacrificial layer at 2,400 rpm / 60 s (10 μm) on a 2 mm thick glass plate. And Ecoflex 00-50 (Smooth-On Inc.), as a substrate material, was spin coated on the photoresist layer. The part A and B of Ecoflex 00-50 were mixed at 1:1 and poured on the photoresist layer (Figure 3(a)). After the air bubbles in Ecoflex were removed using a vacuum pump, the Ecoflex layer was spin coated at 1,000 rpm / 60 s (70 μm). At this time, if the time, taken from the mixing of part A and B to the spin coating, was more than 10 minutes, the Ecoflex is cured and it affects the spin coating of the thin Ecoflex layer. The spin-coated Ecoflex layer was cured at room temperature for 30 minutes. Next, a polyimide film mask (25 μm), patterned with a laser cutting method, was placed on the cured Ecoflex layer, and it was placed on a hot plate at 85 $^{\circ}\text{C}$ for the CNT spray coating.

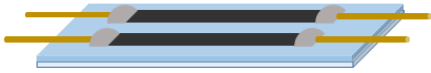
For the spray coating of the CNT thin film, a CNT spray solution needs to be prepared in advance. Commercial 3wt% multi-wall carbon nanotube (MWCNT) water dispersion (US Research Nanomaterials Inc., outer diameter: 20-30 nm, length: 10-30 μm) of 3 mL was diluted in isopropyl alcohol (IPA) of 110 ml at 0.1wt%. And it was sonicated for 1 hour at room-temperature. During this process, the temperature should not exceed 35 $^{\circ}\text{C}$. Next, the CNT spray solution was sprayed on the Ecoflex layer and the polyimide mask, on the 85 $^{\circ}\text{C}$ hot plate, such as Figure 3(b) (spray pressure: 2.4 bar, flow rate: 10 mL/min). After spraying, the polyimide mask was removed from the Ecoflex layer, and the sensor was cleaned with IPA. At this time, we have to be careful not to fall the CNT thin film, because the adhesion of the Ecoflex layer and CNT thin film is weak, yet. After the cleaned sensors were placed on the hot plate for 10 minutes, it was thermal-annealed in convection oven at 150 $^{\circ}\text{C}$ for 30 minutes. This step was for enhancing the adhesion of the Ecoflex layer and the CNT thin film.



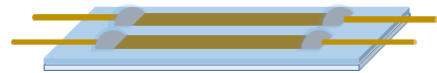
(a) Ecoflex Spin Coating



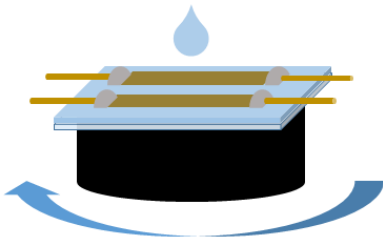
(b) CNT Spray Coating and Annealing



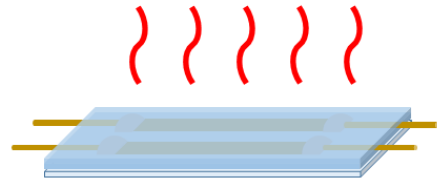
(c) Soldering Wire with Silver Paste



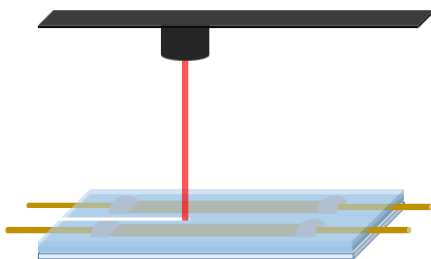
(d) Electrodeposition of AuCNT Composites



(e) Ecoflex Spin Coating (2nd Layer)



(f) Curing in Oven



(g) Laser Cutting



(h) Releasing

Figure 3. Fabrication process of strain sensors.

Copper wires with a length of 4 cm were bonded on the exposed CNT thin film using silver paste (Figure 3(c)). And this area was sealed with silicone elastomer (Kwik-sil, World Precision Instruments), to prevent the breakage of the silver paste during stretching.

Next, we deposited the AuCNT composites on the CNT thin film using an electrodeposition method. For this method, we had to prepare an electrodeposition solution. Short MWCNT powder (US Research Nano-materials Inc., outer diameter: < 7 nm, length: 0.5-2 μm) was dispersed in a commercial gold plating solution (TSG-250, Transene company Inc.) at 1 mg/mL, and the solution was sonicated for 1 hour [25]. A gold wire and the sensors were connected to anode and cathode of pulse generator, respectively, and the device was inserted into the 3D-printed frame (Figure 4(a)). The inner width of the frame is 5 cm, and the distance between the center of the sensors and the gold wire is about 4.8 cm (Figure 4(b)). And then, we put the electro-deposition solution into the frame. After that, monophasic pulse (1.5 V, 1 Hz, 50 % duty cycle) was applied for 8 minutes. The silicone elastomer surrounding the silver paste also prevents that the AuCNT composites was deposited on the silver paste which is relatively more conductive than the CNT thin film.

Next, second Ecoflex layer (70 μm) was spin coated (Figure 3(e)), and was cured in the convection oven at 70 °C for 2 hours (Figure 3(f)). After the curing of the second Ecoflex layer, the sensor's shape was patterned by a laser-cutting system. (Figure 3(g)). Finally, we released the sensors from the glass plate by dissolving the sacrificial layer, AZ 9260, in acetone (Figure 3(h)).

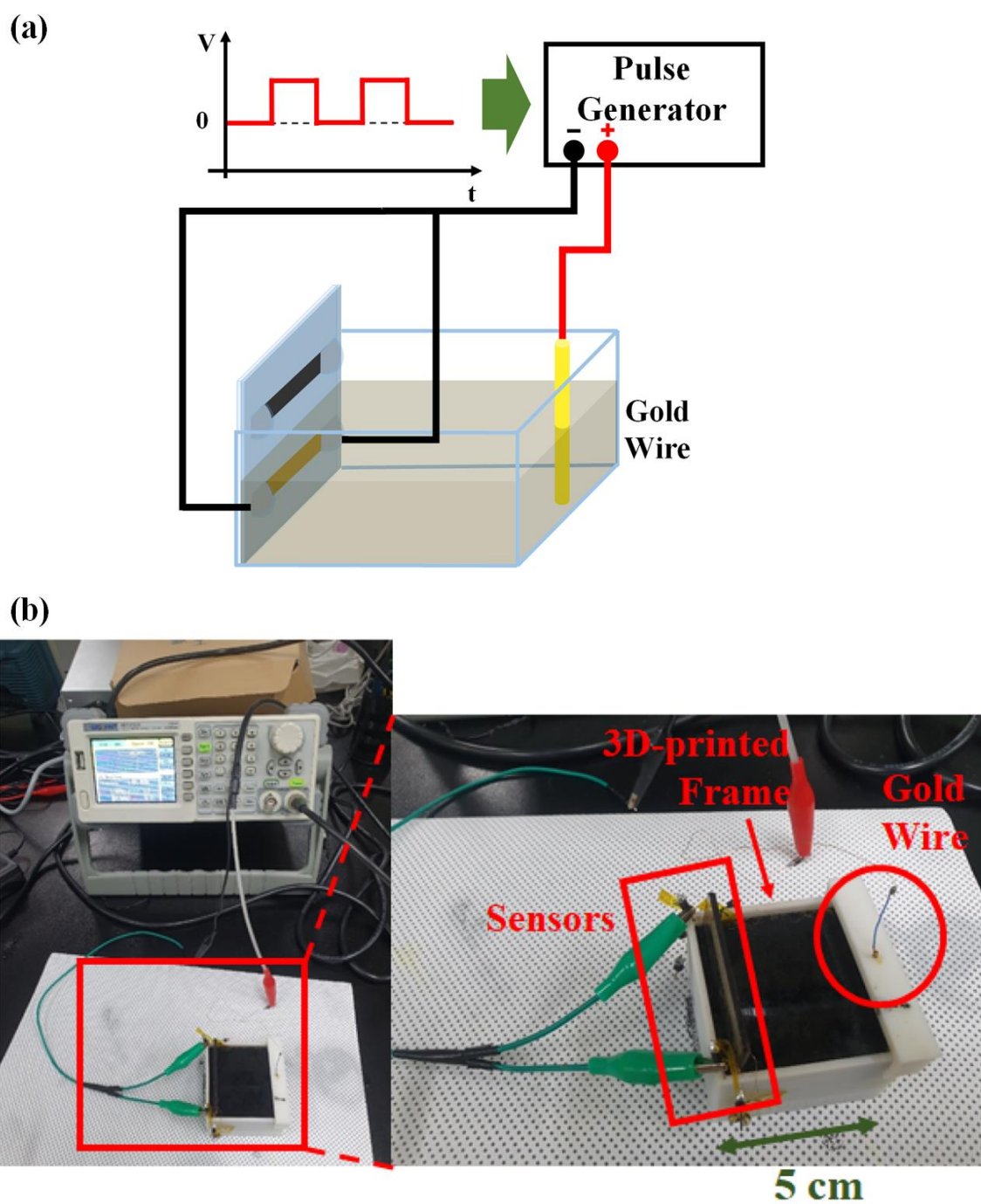


Figure 4. Electrodeposition of AuCNT composites. (a) The conceptual figure of electrodeposition. (b) The electrodeposited sensor with the pulse generator.

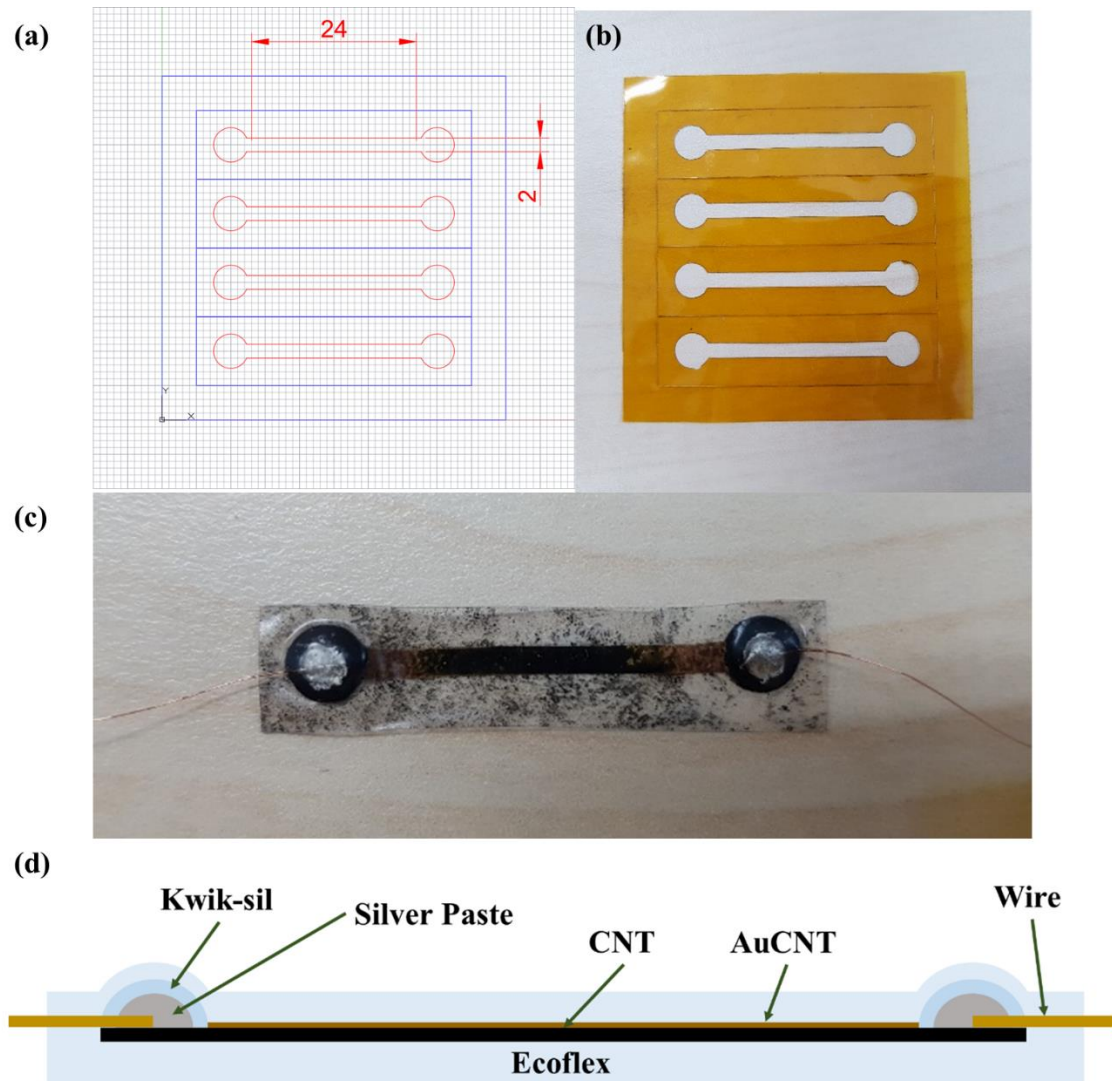


Figure 5. AuCNT strain sensor. (a) The CAD image of stick-shaped sensor design. (b) Polyimide film mask for CNT patterning. (c) The AuCNT strain sensor fabricated with above process. (c) Cross-section image of the AuCNT strain sensor.

Figure 5(a) and (b) shows the CAD design of the stick-shaped sensors and the polyimide film mask for the patterning of CNT thin film. We used a commercial polyimide film. Figure 5(c) is the sensor fabricated by the above process, and Figure 5(d) shows a cross-sectional view of the sensor.

2.2 Strain-Resistance Measurement

The resistance according to strain to evaluate the performance of sensors was measured. For this, we developed a measurement platform using an Arduino, a motor, and a distance sensor. We used the law of voltage division for measuring the resistance of the sensors (Figure 6(a)). A detecting resistor we used was 100 k Ω resistor. And we calibrated the difference between the ideal value of the detecting voltage and the actual input signal of the Arduino. We used 10 k Ω , 100 k Ω , 1 M Ω resistors and measured the actual input voltage of the Arduino. And we matched two values on the code. Furthermore, considering the noise of the Arduino input signal, 200 signals were read and averaged when measuring resistance at one time.

We used the motor to extend and contract the sensor. And we also used the infrared distance sensor (GP2Y0A41SK0F) for detecting the length of the sensor, the motor drive (L298N) for switching the extending and contracting of the sensor by switching of the direction of rotation of the motor when the sensor reaches the desired length. Furthermore, the measured data was stored on the SD card as a text file by the SD card module. Figure 6 (b) and (c) show our strain-resistance measurement platform.

Using this platform, we repeatedly measured the resistance changes within 200% strain over 40 cycles. The speed of strain change was 200 % strain / min, and the resistance was measured at every 20% strain step. The performance of each sensor was specified as an average of later 10 cycles.

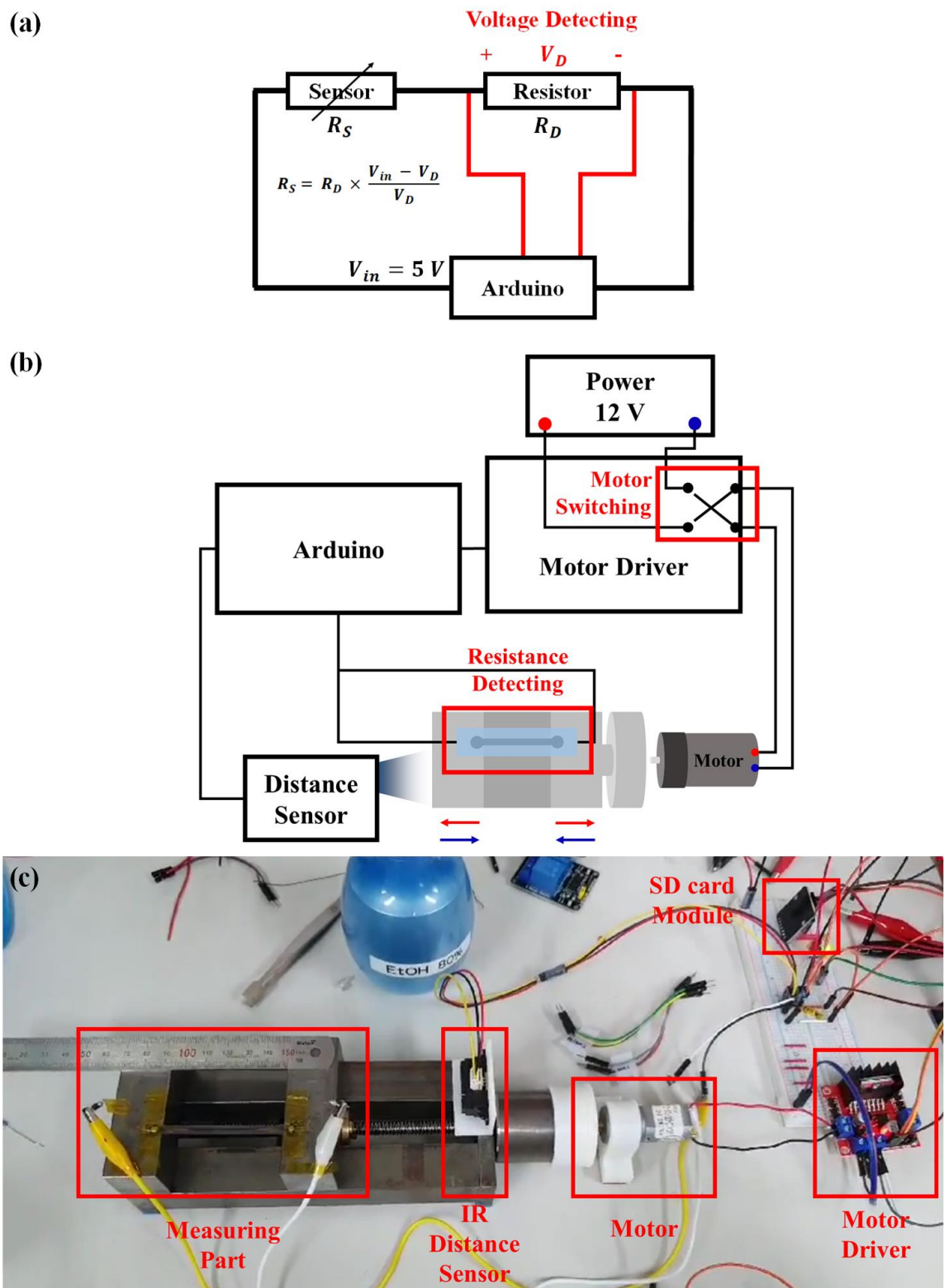


Figure 6. Strain-Resistance measurement. (a) Resistance detecting with the voltage division law. (b, c) Measurement platform with Arduino.

2.3 Volume-Resistance Measurement

The objective of this study is to develop the strain sensors to be applied to the bladder monitoring. Therefore, we need to measure resistance changes of the strain sensors according to the volume with a balloon or a bladder. So, we developed a measurement platform, that can measure the resistance characteristics according to the volume, using Arduino, pumps, and flow sensors.

We used two water pumps (HS-WATER PUMP IV), two solenoid valves (HDW-2120), and two flow sensors (YF-S401) since we need both flow-in line and flow-out line. And we connected the two lines using a T-shaped tube. Next, the two lines were connected in parallel to the output terminals of the motor driver (L298N). And when the amount of water measured in the flow sensor reached the desired level, the Arduino signaled the motor driver to change flow-in and flow-out (Figure 7).

The resistance measurement method is the same as described in the section of 2.2. Similarly, we used a detecting resistor of 100 k Ω , and calibrated the difference between the ideal value of the detecting voltage and the actual input signal of the Arduino using 10 k Ω , 100 k Ω , and 1 M Ω resistors. In this system, the water flow rate is 10 mL/s.

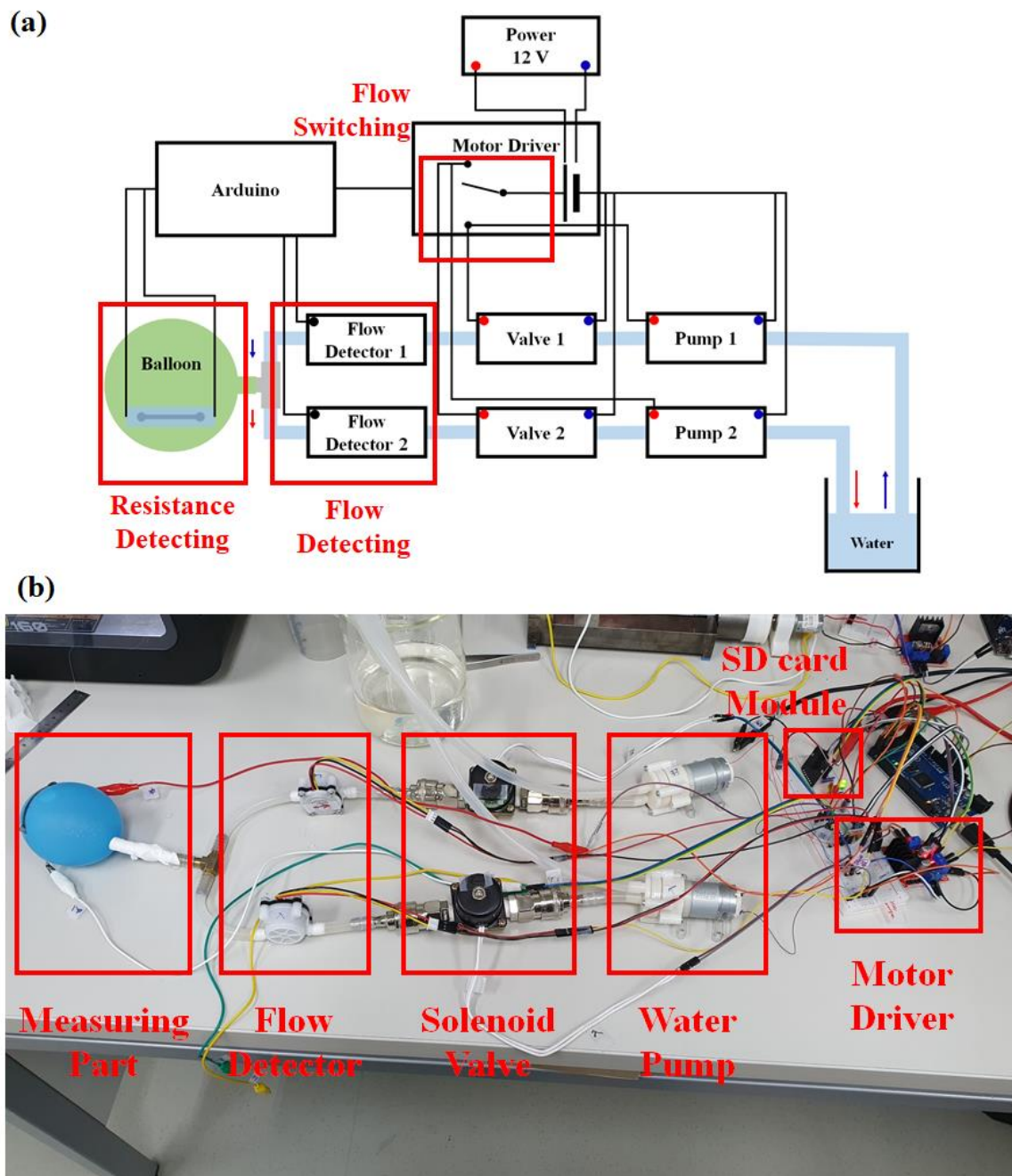


Figure 7. Volume-Resistance measurement platform with Arduino.

2.4 Balloon-Model Test

We measured the resistance according to volume by applying our sensor to a balloon-model with a diameter of 5 cm before applying it to the bladder. In this test, we used sensors that had previously performed 40 cycles of strain test.

The sensors were fixed on the balloon using a double-sided tape. We attached the tape to the bottom of the silicone elastomer surrounding the silver paste. And we measured the resistance characteristics within the volume of 200 mL. We measured the resistance every 10 mL of a volume and repeated it 10 cycles. And the performance was specified as an average of later 5 cycles.

2.5 Volume Monitoring

We also developed a monitoring system that shows the state of the volume, using Arduino and 3 LEDs. Also, this system was applied to the balloon-model. The result of the resistance characteristics according to the volume measured in the section of 2.4 was used in this system. The green, yellow, and red LEDs are sequentially turned on, when the volume of the balloon increase as 50 mL, 100 mL, and 150 mL.

The resistance measurement method was the same as described in the section of 2.2. And the resistance value of the sensor when the Arduino was first operated was set to R_0 . After that, the resistance was then repeatedly measured to calculate R/R_0 , which determined whether the LED was turned on or off.

2.6 *Ex-vivo* Test with Pig's Bladder

We also applied our sensors in the extracted pig's bladder. The sensor was fixed to the bladder wall using surgical suture (SK434, Black silk 4-0, AILEE CO., LTD). We sutured the Ecoflex part of the strain sensors around the wire bonding section with the bladder wall. And the silicone elastomer, such as the one surrounded around the silver paste, was used to prevent the sutured part from tearing when the sensor was stretched.

We measured the resistance according to the volume during the expansion of the bladder using a measurement platform as described in the section of 2.3. 600 mL of water was injected into the bladder and the resistance of

the sensors was measured by every 20 mL. The length of the sensor at the maximum volume of the bladder was measured to determine how stretched the bladder wall was. However, since the extracted bladder cannot contract the muscles of the bladder wall, it is impossible that the bladder returns to its original size. Therefore, we only attempted one measurement for one bladder.

2.7 3-Channel Strain Sensor

We designed a 3-channel strain sensor that can track the expansion direction of the bladder wall (Figure 8). This 3-channel strain sensor was developed using the same fabrication process as described in the section of 2.1. We measured the resistance characteristics of each channel of this sensor according to the volume with the balloon-model and the pig's bladder in the same way described in the section of 2.4 and 2.6. We used the measurement platform described in the section of 2.3 and this platform was developed to allow the resistance of 3 channels to be measured simultaneously via parallel connections.

In this 3-channel strain sensor, the AuCNT composites were plated separately for each channel. Because the AuCNT strain sensor was fabricated using the electrodeposition method, it was very difficult to control randomly deposited composites, as well as gauge factor of each channel. Therefore, we used the following method to indirectly determine the expansion of each channel of the 3-channel strain sensors.

$$\frac{\Delta R_n/R_{0,n}}{GF_n}$$

In this formula, n is channel number.

We also represent the relative expansion of each channel. It was assumed that when the resistance is R_0 , the relative expansion is 1.

$$\frac{\Delta R_n/R_{0,n}}{GF_n} + 1$$

Each channel's gauge factor was calculated respectively by measuring resistance at 0 %, 100 %, and 200 % using a multimeter, after 20 times of stretching in ~200 % strain of each channel.

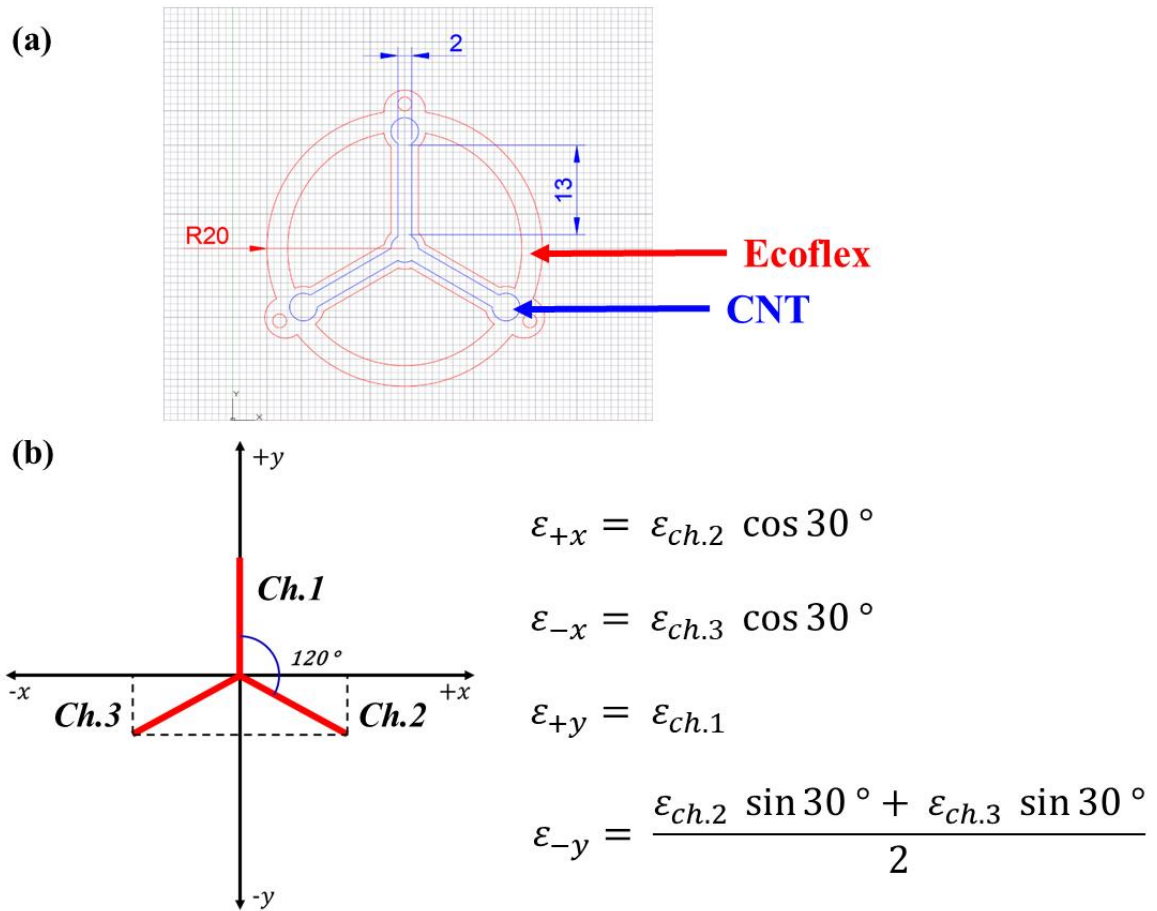


Figure 8. 3-channel strain sensor. (a) Design of 3-channel strain sensor. (b) Concept for detecting of expansion direction with 3-channel strain sensor.

III. RESULTS AND DISCUSSION

3.1 Fabrication Conditions of CNT Strain Sensor

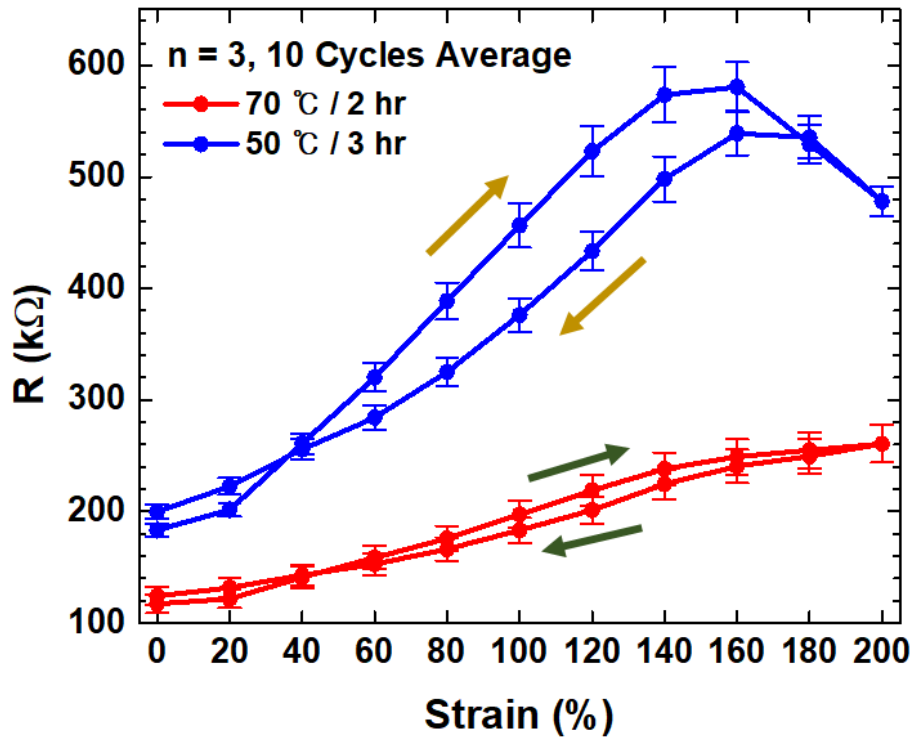
We experimented to optimize several process conditions to develop an Ecoflex-CNT strain sensor. In this chapter, we compare the characteristics of the CNT strain sensors depending on the curing temperature of the second Ecoflex layer and the amount of CNT sprayed. These two conditions most affect the performance of the strain sensor.

First, we compared the performance of the strain sensors according to the curing temperature of the second Ecoflex layer. Curing temperatures of liquid Ecoflex have been known to affect the formation of Ecoflex-CNT nanocomposites [18]. The strain sensors were fabricated in three cases, with the curing temperatures of 50 °C, 70 °C, and 85 °C, respectively, and the fabrication conditions other than curing temperature were all the same as described in the section of 2.1. Figure 9 shows the resistance characteristics of the CNT strain sensors with the curing temperature of 50 °C and 70°C, within 200 % strain ranges. The sensors with the curing temperature of 50 °C showed the smallest resistance value of $183 \pm 30 \text{ k}\Omega$ ($n = 3$) at 0 % strain, and the largest value of $581 \pm 123 \text{ k}\Omega$ ($n = 3$) at 160 % strain. Also, the sensors with the curing temperature of 70 °C showed the smallest resistance value of $117 \pm 46 \text{ k}\Omega$ at 0 % strain, and the largest value of $261 \pm 92 \text{ k}\Omega$ at 200 % strain. And the maximum rate of resistance change was 3.16 ± 0.37 ($n = 3$) and 2.25 ± 0.16 ($n = 3$) with the curing temperatures of 50 °C and 70 °C, respectively. The resistance change rate of the sensors with the curing temperature of 50 °C was higher than the sensors with the curing temperature of 70 °C. However, the maximum point of the resistance change with the curing temperature of 50 °C was 160 % strain. Therefore, it is not suitable for the strain sensor in the range of 200 % strain. Also, in case of the sensors with curing temperature of 85 °C, it was impossible to measure the resistance characteristics since the strain sensor was opened even in a small strain. So, we determined that the curing temperature of 85 °C was also not suitable for the strain sensor in the range of 200 % strain. Therefore, we determined that the curing temperature of 70 °C was the most suitable condition for fabrication of our sensors.

Next, we investigated the performance of the strain sensors according to the amount of CNT sprayed. We compared the characteristics of the CNT strain sensors depending on the amount of MWCNT water dispersion where the CNT solution was 1.5 mL and 3 mL, respectively. Because the density of the CNT spray solution

was the same at 0.1 wt%, the amount of CNT spray solution for the latter case was twice as large as that of the former. Figure 10 shows the resistance characteristics of the CNT strain sensors according to the amount of CNT dispersion. The sensors with MWCNT water dispersion 1.5 mL showed the smallest resistance value of $893 \pm 49 \text{ k}\Omega$ ($n = 1$, 10 cycles average) and the largest value of $2030 \pm 107 \text{ k}\Omega$ ($n = 1$, 10 cycles average) at 200 % strain. Also, the sensors with MWCNT water dispersion 1.5 mL showed the smallest resistance value of $117 \pm 46 \text{ k}\Omega$ ($n = 3$) and the largest value of $261 \pm 92 \text{ k}\Omega$ ($n = 3$) at 200 % strain. And the maximum rate of resistance change was 2.28 ± 0.20 ($n = 1$, 10 cycles average) and 2.25 ± 0.16 ($n = 3$) with MWCNT water dispersion 1.5 mL and 3 mL, respectively. These are very similar values. However, the resistance value in 1.5 mL case was about 7 times higher than 3 mL case, and this value is difficult to distinguish when the network of the strain sensor is broken. Therefore, we determined that the 3 mL of MWCNT water dispersion was the most suitable condition for fabrication of our sensors.

(a)



(b)

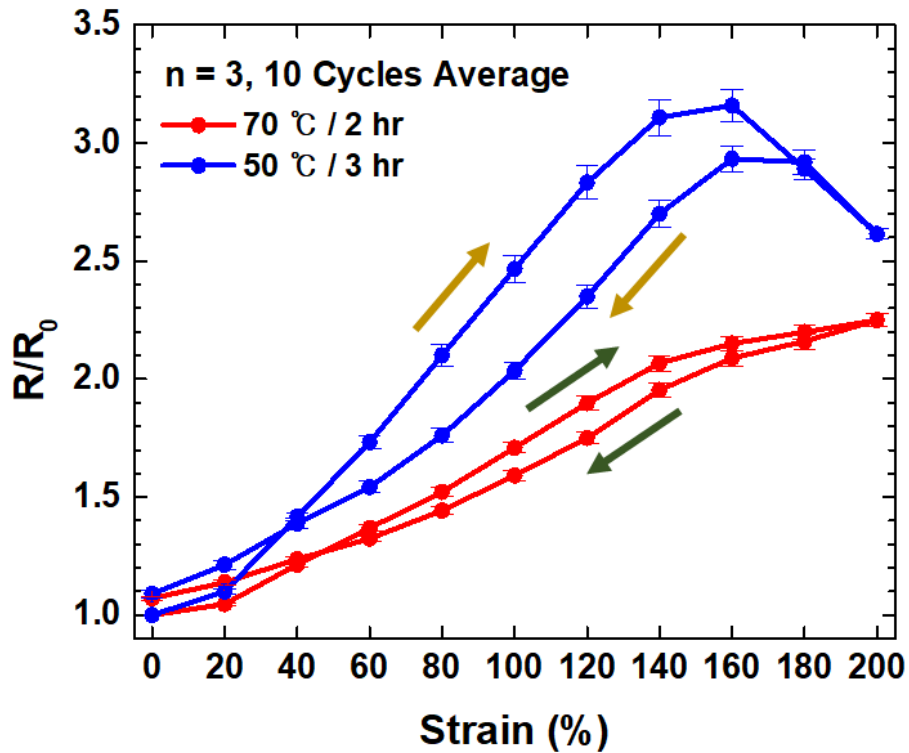


Figure 9. Comparison of characteristics of the CNT strain sensor by curing temperature between 50 °C and 70 °C. (a) The resistance and (b) the resistance change rate according to the strain.

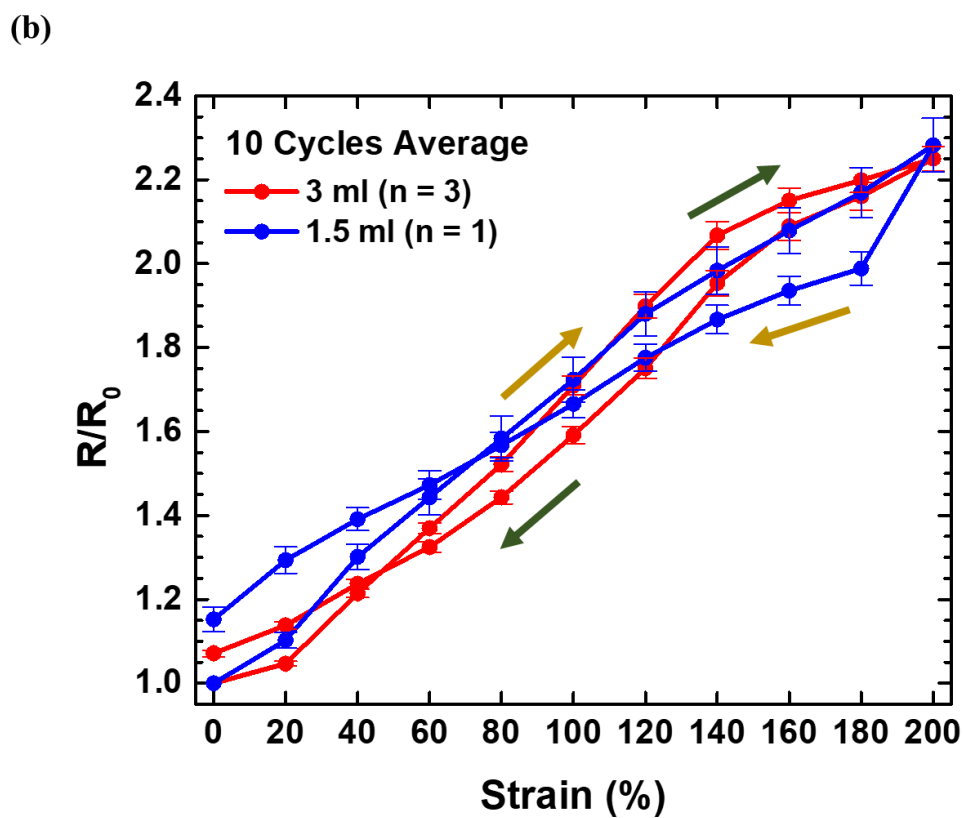
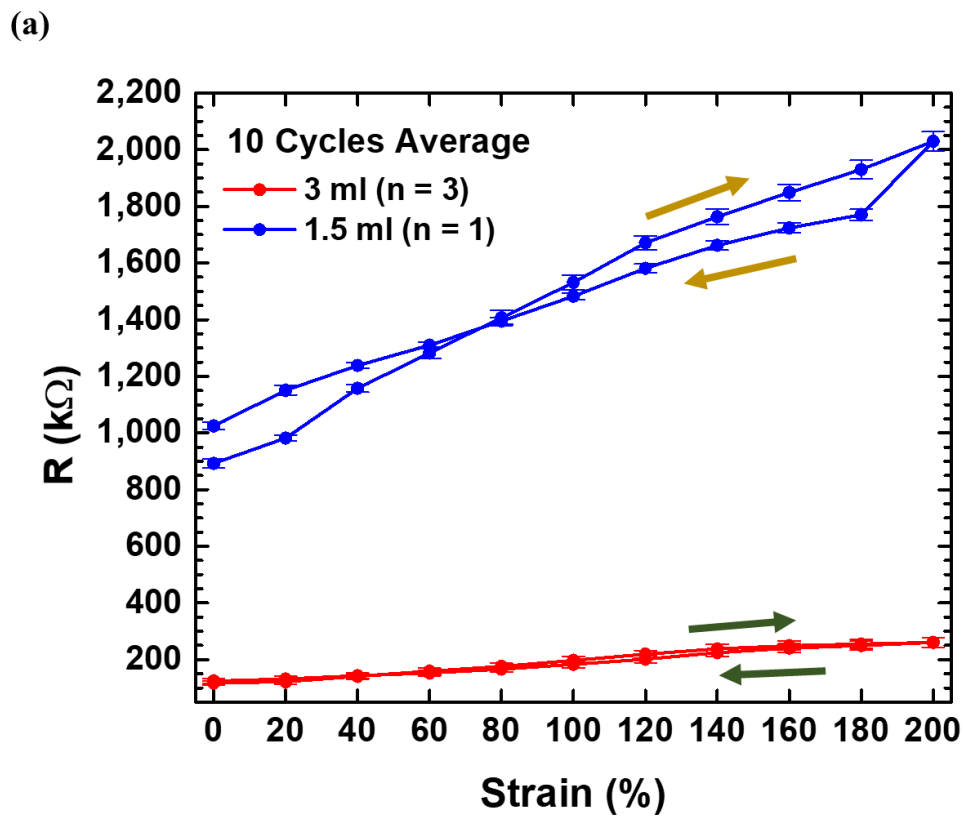


Figure 10. Comparison of characteristics of the CNT strain sensor by amount of CNT water dispersion. (a) The resistance and (b) the resistance change rate according to the strain.

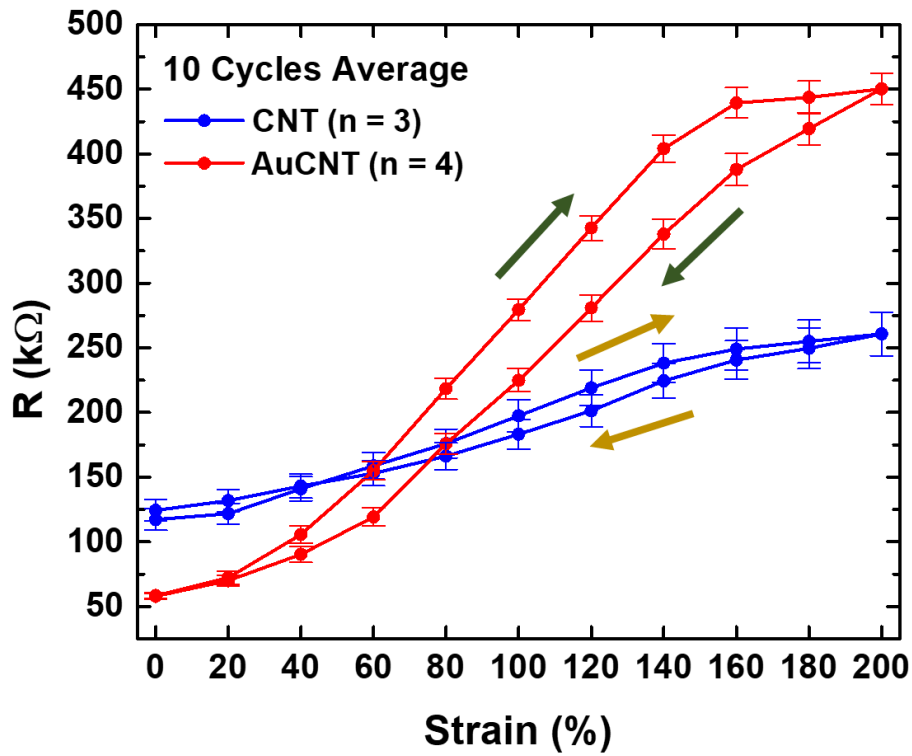
3.2 Comparison of CNT and AuCNT Strain Sensor

To increase sensitivity of our Ecoflex-CNT strain sensors, AuCNT composites were additionally deposited on the CNT film using the electrodeposition method. Fabrication conditions other than the additional deposition of the AuCNT composites are same way as the conditions optimized in the section of 3.1. Then, we compared the resistance characteristics of the strain sensors fabricated with only CNT and the additional deposition of AuCNT composites.

Figure 11 shows the results of measuring the resistance characteristics of two type sensors, within the strain range of 200 %. As a result, the strain sensors with only CNT showed the resistance value, $117 \pm 46 \text{ k}\Omega$ ($n = 3$) at 0 % strain and $261 \pm 92 \text{ k}\Omega$ ($n = 3$) at 200 % strain. And then, the strain sensors with the AuCNT composites showed the resistance value, $58 \pm 14 \text{ k}\Omega$ ($n = 4$) at 0 % strain and $450 \pm 77 \text{ k}\Omega$ ($n = 4$) at 200 % strain. These strain sensors also showed the maximum rate of resistance change, 2.25 ± 0.16 ($n = 3$) and 7.89 ± 0.93 ($n = 4$) at 200 % strain. And gauge factors of these strain sensors were calculated as 0.625 ± 0.073 ($n = 3$) and 3.455 ± 0.463 ($n = 4$), respectively. This result indicates that the gauge factor of the strain sensors with AuCNT composites was improved by about 5 times than that of the sensor with the CNT, and the initial resistance was 2 times lower. As a result, we demonstrate that the deposition of the AuCNT composites improves the sensitivity of the Ecoflex-CNT strain sensors within the strain range of 200 %.

Figure 12 and 13 show cross-sectional SEM images of the CNT strain sensor and the AuCNT strain sensor. In Figure 12, the overall thickness of the CNT strain sensor was about $130 \mu\text{m}$ and the thickness of the CNT thin film between the Ecoflex layer was about $5 \mu\text{m}$. Also, according to Figure 13, the thickness of the CNT thin film and the AuCNT composites formed between the Ecoflex layers in the AuCNT strain sensor is approximately $8 \mu\text{m}$. In this image, we could see that CNT and Au particles were mixed between the Ecoflex layers. Furthermore, we were able to confirm that the size of Au particles was about $1 \mu\text{m}$.

(a)



(b)

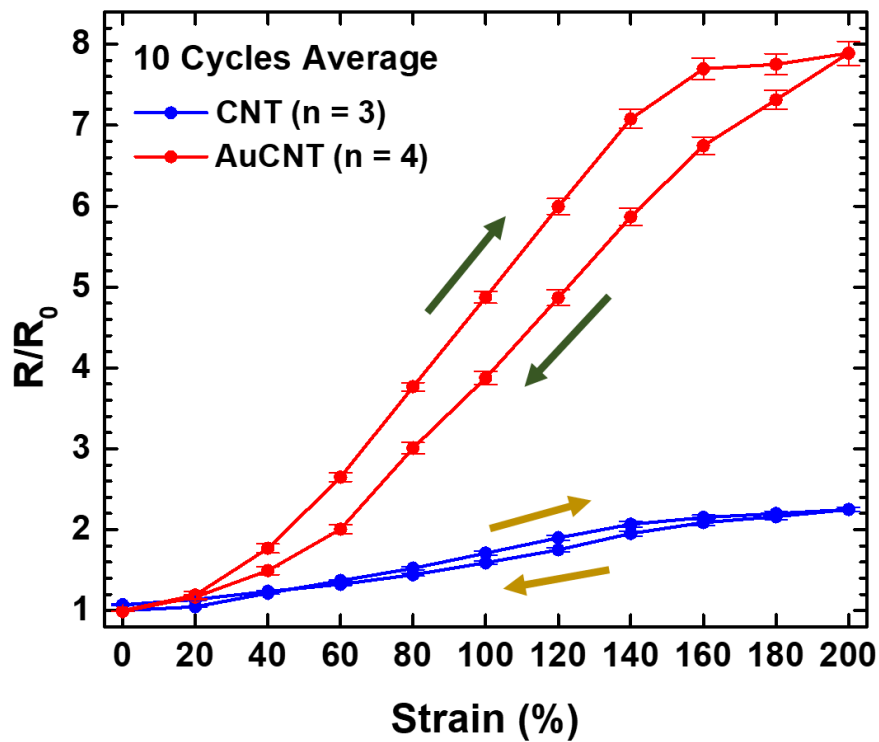


Figure 11. The comparison result of the CNT strain sensors and AuCNT strain sensors. (a) The resistance and (b) the resistance change rate according to the strain.

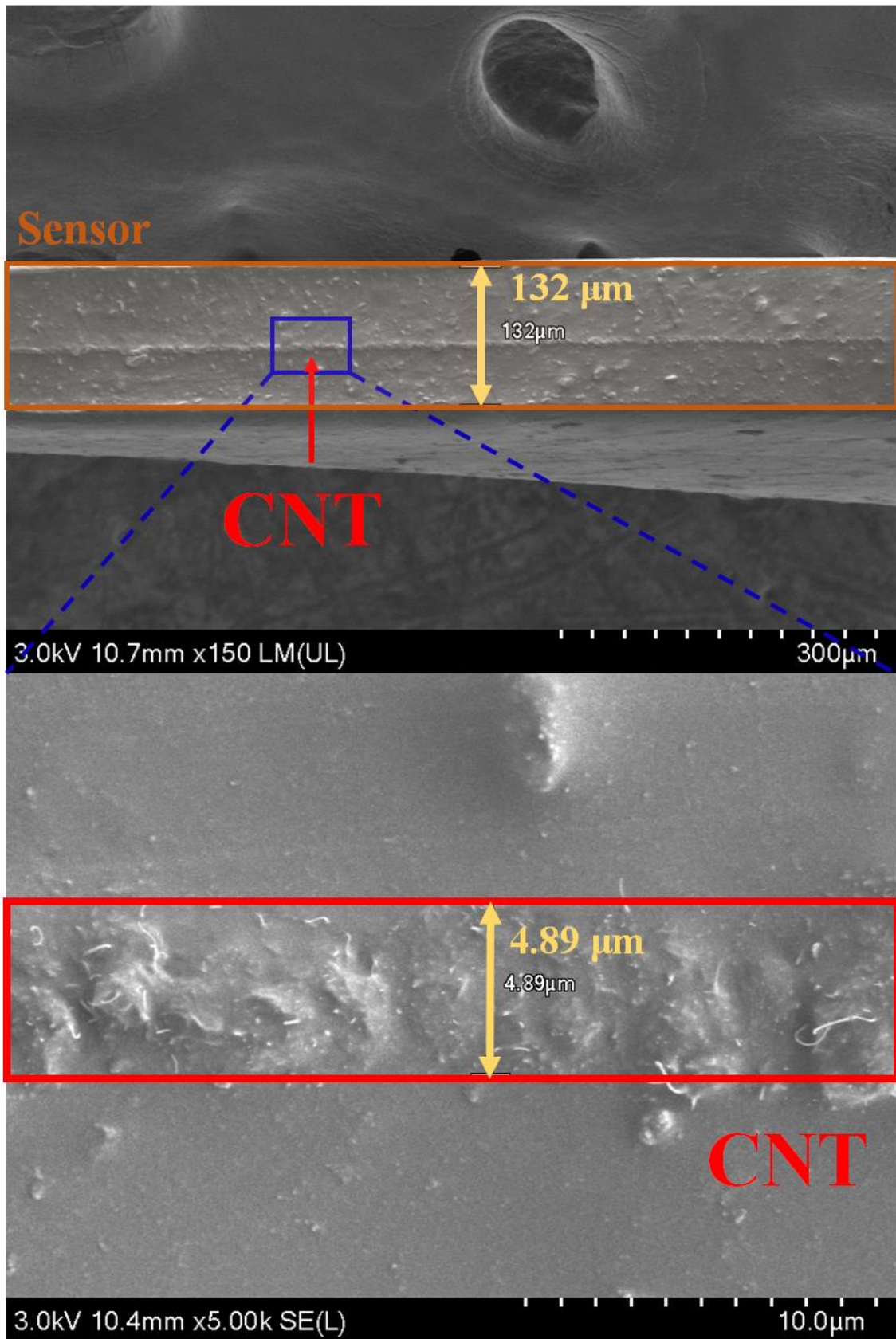


Figure 12. Cross-section SEM images of the CNT strain sensor.

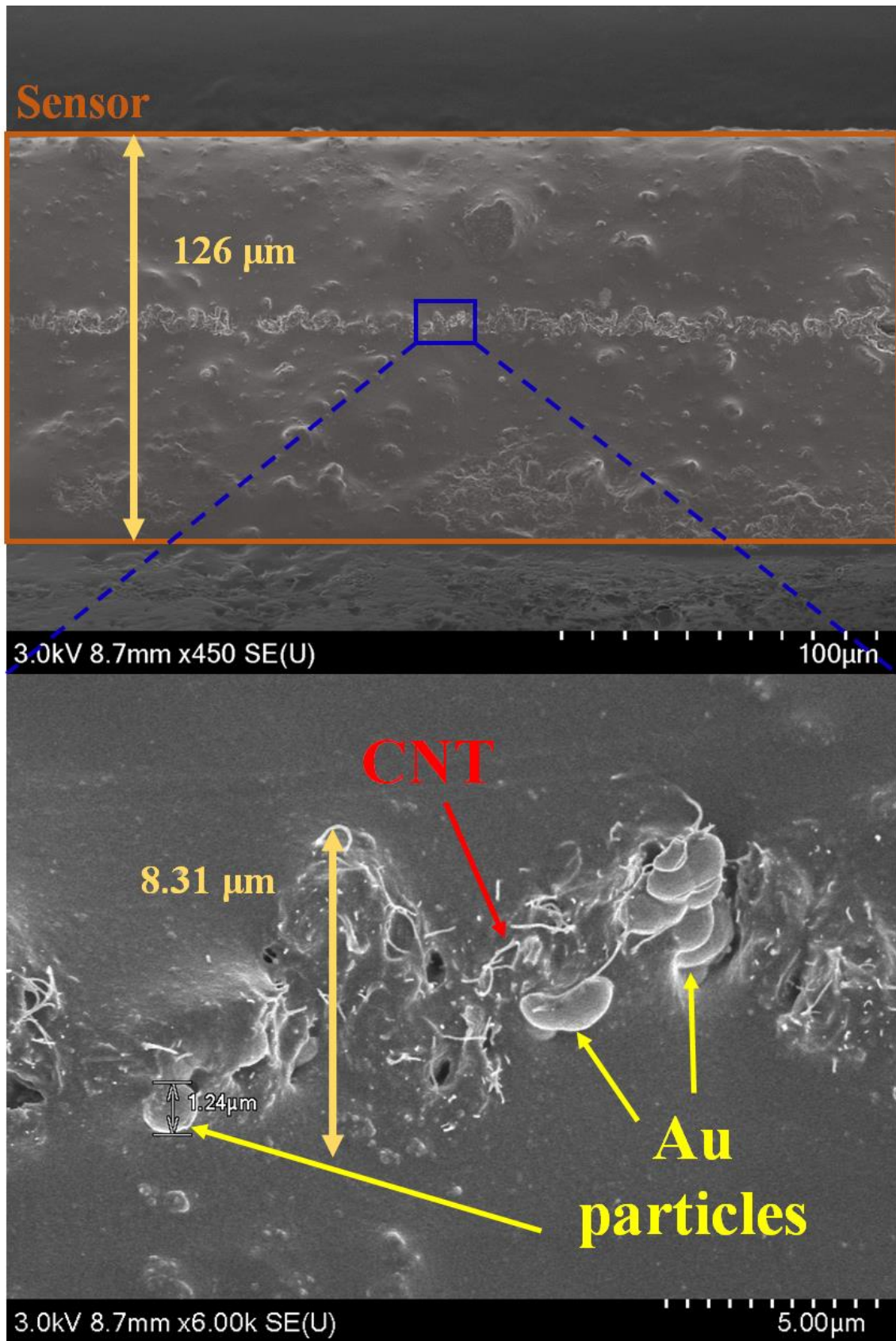


Figure 13. Cross-section SEM images of the AuCNT strain sensor.

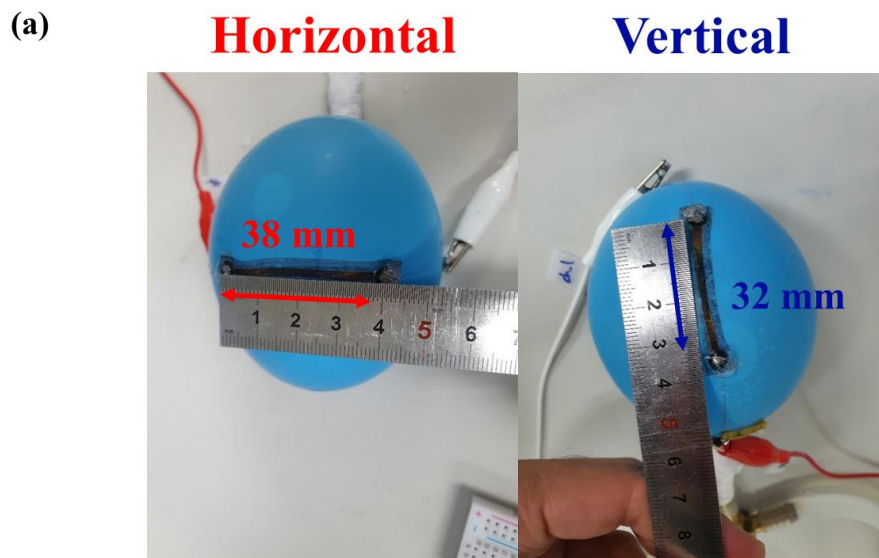
3.3 Balloon-Model Monitoring

Next, we applied the AuCNT strain sensors, which completed the resistance characteristic measurements in the section of 3.2, to the balloon-model to investigate their performance for volume monitoring before applying them to pig's bladders.

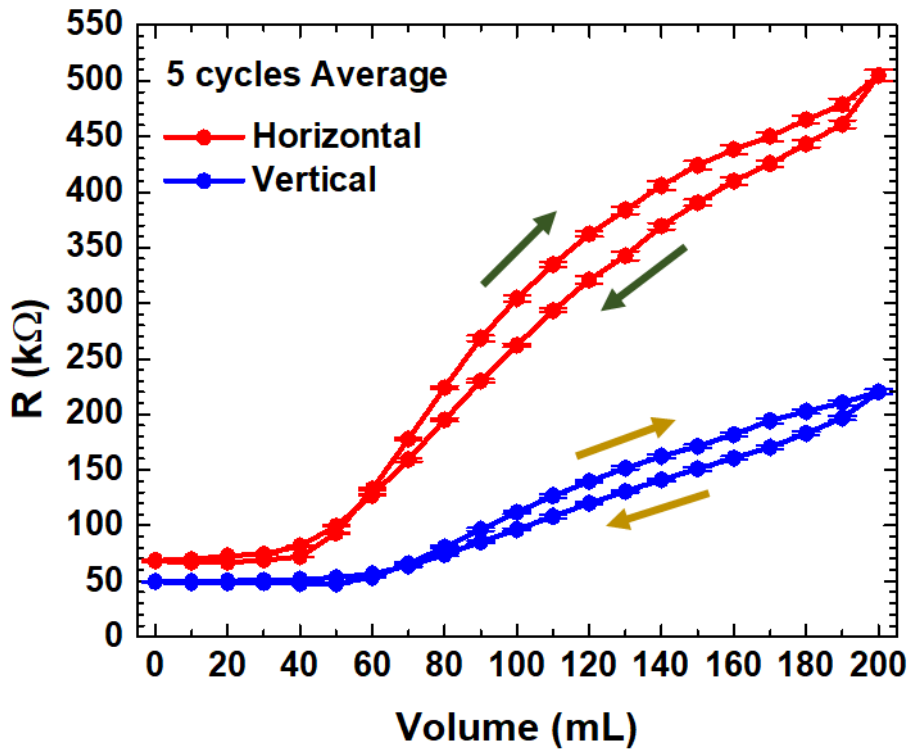
Figure 14(a) shows a strain sensor attached to a balloon wall. We attached the same sensor to the same balloon in two directions, horizontally and vertically, to measure the resistance characteristics according to the volume. With Figure 14(a), at 200 mL of the volume, the lengths of the strain sensor stretched were 38 mm (90 % strain) in horizontal, and 32 mm (60 % strain) in vertical. In this result, we confirm that the balloon we used stretched more in the horizontal direction.

Figure 14(b) and (c) are the results of measuring the resistance characteristics according to the volume of the balloon with the strain sensor as seen in (a). In Figure 14(c), the resistance change rate at 200 mL in the two case were 7.40 ± 0.11 (5 cycles average) in the horizontal, 4.45 ± 0.04 (5 cycles average) in vertical. As a result of the repeated measurements, the standard deviation of the values measured in 5 cycles was within 2 % of the average value. Therefore, we demonstrate that our sensors can measure the volume of the balloon repeatedly and reliably.

Furthermore, we have seen that as the balloon expands, the balloon wall stretches more in the horizontal direction. And these results are same with the direct measurement of the stretched length of the strain sensor in Figure 14(a). As a result, we demonstrate that our sensors can measure the expansion of the balloon wall.



(b)



(c)

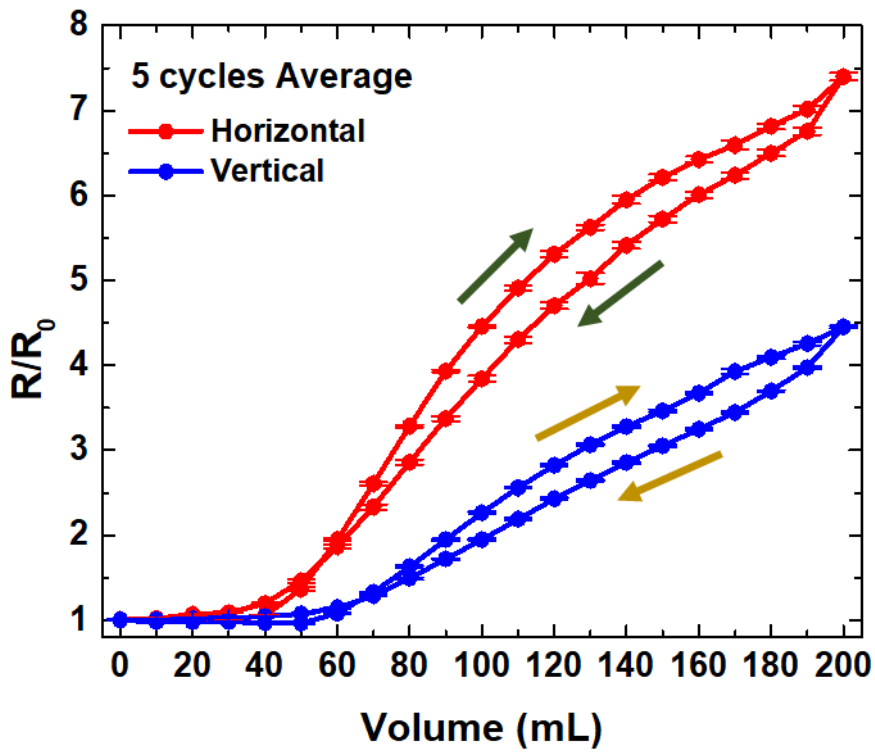


Figure 14. Volume-Resistance measurement in Balloon-Model. (a) The sensor attached on the balloon, horizontally and vertically at 200 mL. (b, c) Characteristics of the sensor according to the volume.

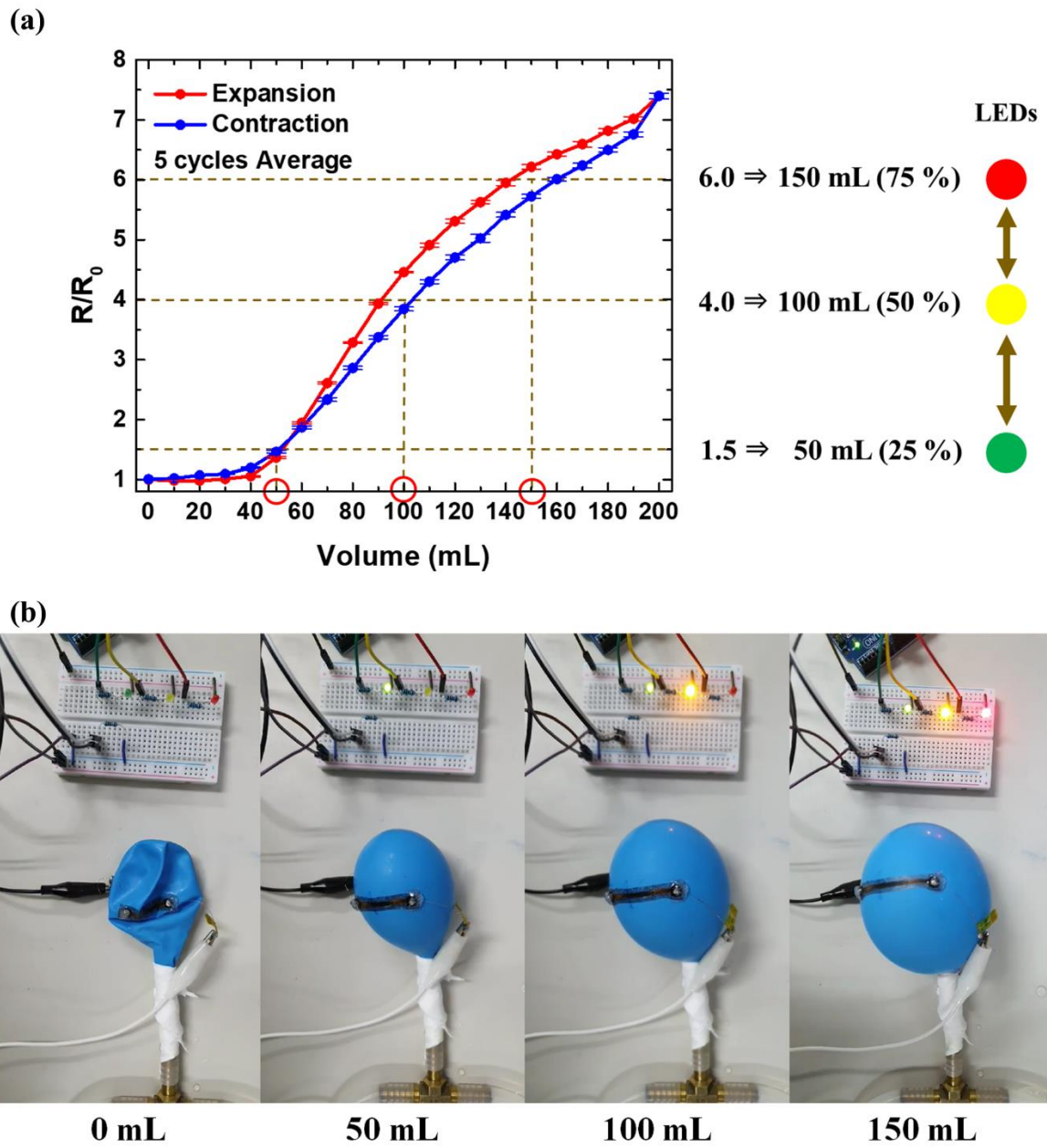


Figure 15. Volume monitoring with Arduino system. (a) Description of the monitoring system using 3-LEDs. (b) Monitoring system with volume of 0, 50, 100 150 mL.

Next, we applied the strain sensor to our volume monitoring system using Arduino and LEDs based on the results of the resistance characteristic according to the volume measured above. We used the result when the strain sensor was attached horizontally, since it is relatively sensitive to volume changes. Figure 15(a) shows the parameters of the monitoring system we used, based on the results of measurement of resistance characteristics according to the volume in horizontal. We used 3 different colored LEDs for this monitoring system. When the volume of the balloon is 50 mL, 100 mL, and 150 mL, the green, yellow, and red LEDs are turned on, respectively, and this is when the resistance change rate of the strain sensor are 1.5, 4.0, 6.0.

Figure 14(b) shows the operating of the monitoring system. We took the video that the LEDs were turned on when the balloon expanded, and calculated the volume of the balloon when each LED was turned on, using video time and flow rate. As a result, we could see that the moment each LED was turned on has an error within 1 second (10 mL). Therefore, we demonstrate that our strain sensor and monitoring system can reliably track the volume of the balloon.

3.4 Ex-vivo Test with Pig's Bladder

Next, we applied our strain sensor to pig's bladder. we attached our strain sensor to the wall of the extracted pig's bladder in order to measure the resistance characteristics according to the volume.

Figure 16 shows a sensor fixed to the wall of a pig's bladder. We found that the sensor attached to the bladder wall with surgical sutures and silicone element was stable at a volume of 600 mL, known as the maximum volume of the pig's bladder. When the volume of the bladder was 600 mL, the sensor was 50 mm long. So, we confirmed that the part of the bladder wall where we attached our strain sensor showed 150 % strain at the volume of 600 mL. In addition, we measured the resistance characteristics of the strain sensor while the volume of the bladder expands to 600 mL. We measured the resistance by attaching the strain sensor horizontally to the center of the bladder, and Figure 17 shows its results. According to the graph in Figure 17(b), when the volume of the bladder expands to 600 mL, the resistance change rate increased to 11.75. We demonstrate that our strain sensors can operate within the 600 mL volume range of the pig's bladder. On the other hand, we found that the result in Figure 16 and 17 showed the higher resistance change rate than the result in the section of 3.2 at same strain of the AuCNT strain sensors. For these results, it is assumed that the pressure from the curvature of the bladder affected the resistance of the strain sensor.

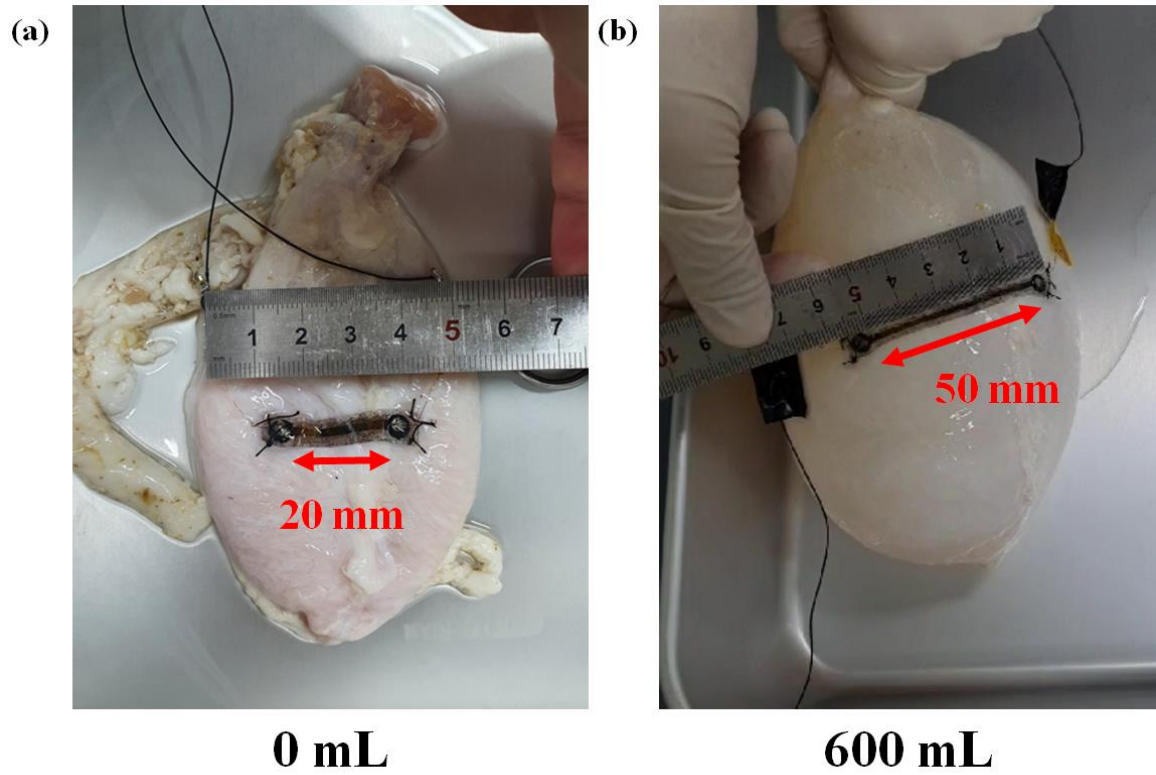
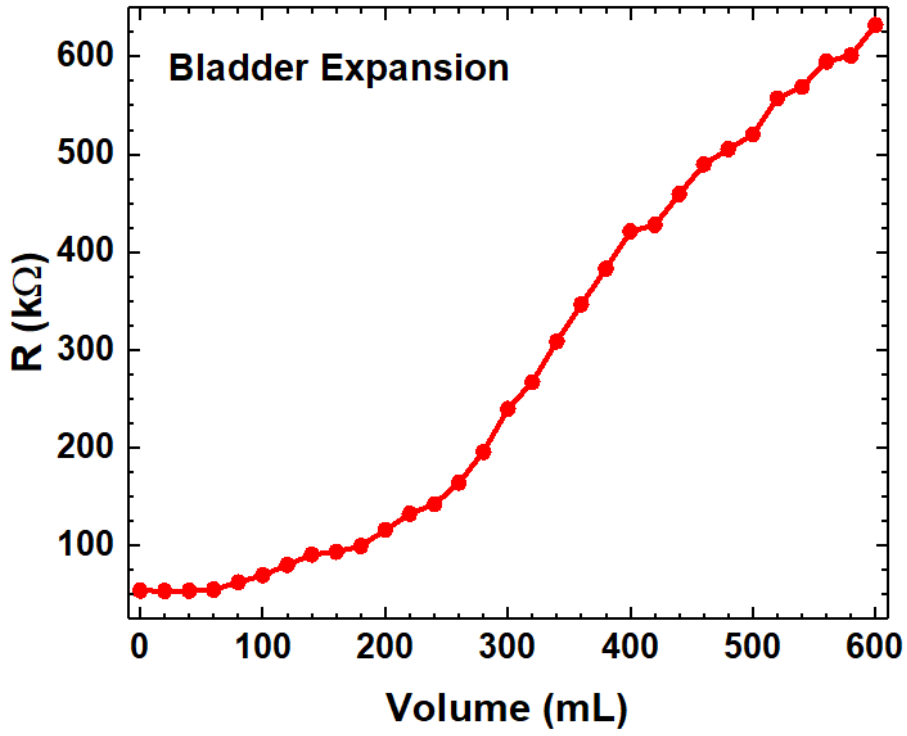


Figure 16. *Ex-vivo* test with pig's bladder. The strain sensor was sutured on the bladder wall. The length of the strain sensor at volume of (a) 0 mL and (b) 600 mL.

(a)



(b)

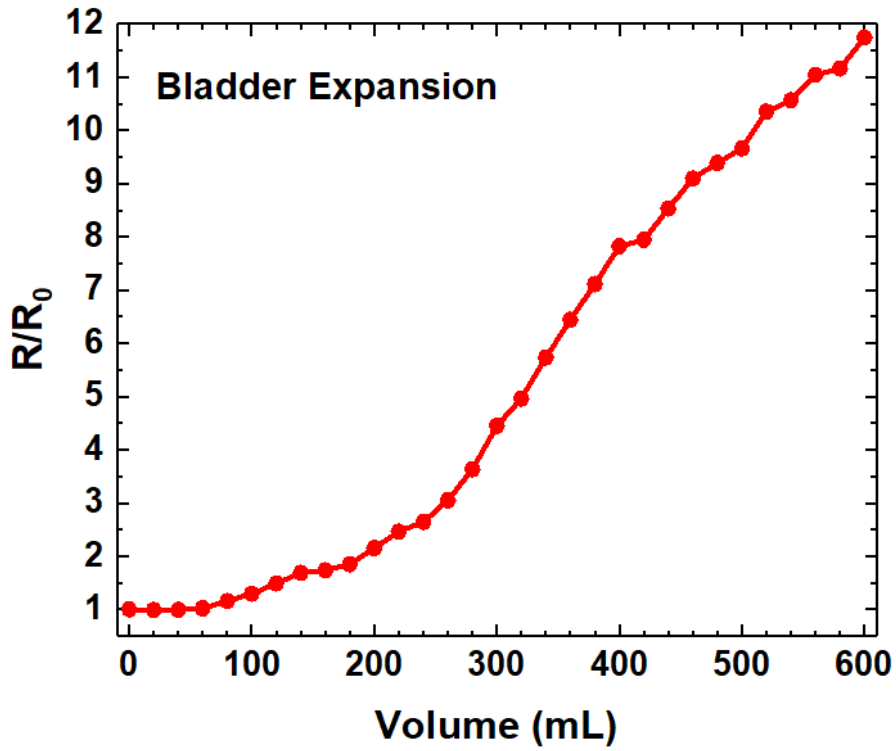


Figure 17. Volume-Resistance characteristics with pig's bladder. (a) The resistance and (b) the resistance change rate according to the volume.

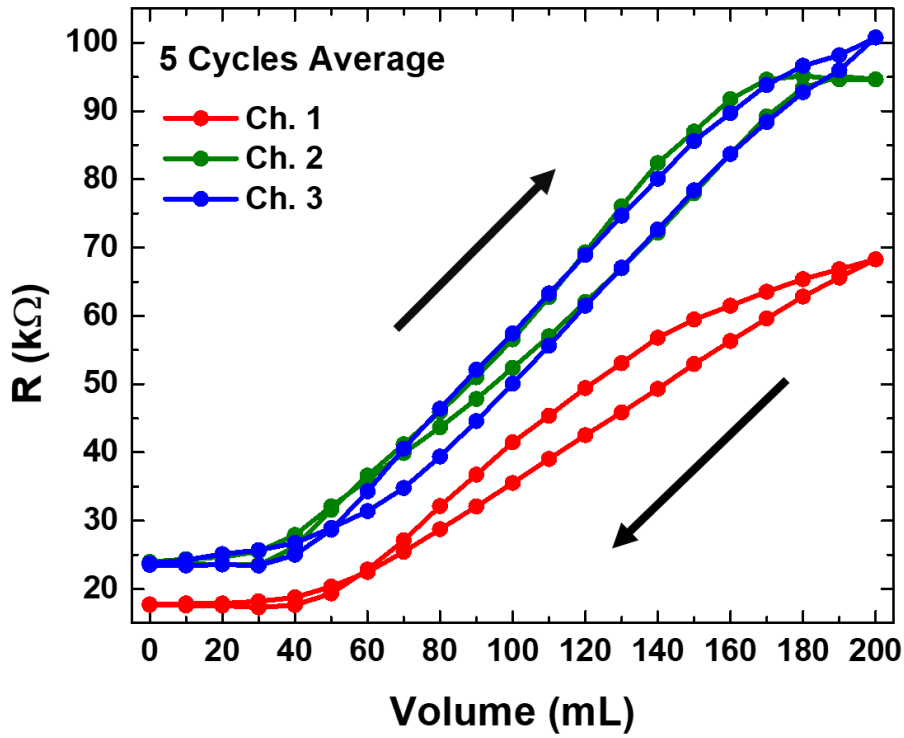
3.5 3-Channel Strain Sensor

We demonstrate that, with prior results, the AuCNT strain sensor we developed can monitor the volume of the bladder through resistance changes. We found that the balloon model has different expansion depending on the direction and this has been also demonstrated in the previous study [2]. Furthermore, we assumed that the pressure from the curvature of the bladder wall affect the resistance of the strain sensor based on the results in the section of 3.4. Thus, we further developed a 3-channel strain sensor that can track the expansion direction of the bladder, not only simply measuring the volume of the bladder. It was also expected that this 3-channel strain sensor would be less susceptible by the pressure from the curvature of the bladder wall be-cause each channel of the 3-channel strain sensor is shorter than the stick-shaped sensors used in previous experiments. Figure 18 shows the 3-channel strain sensor we developed.



Figure 18. The fabricated 3-channel strain sensor.

(a)



(b)

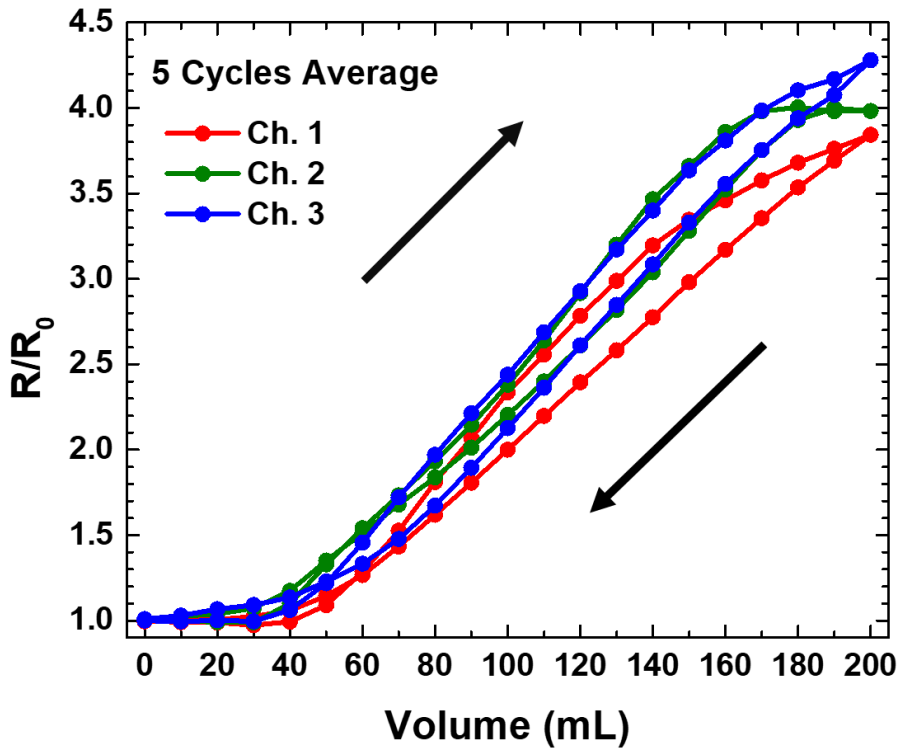
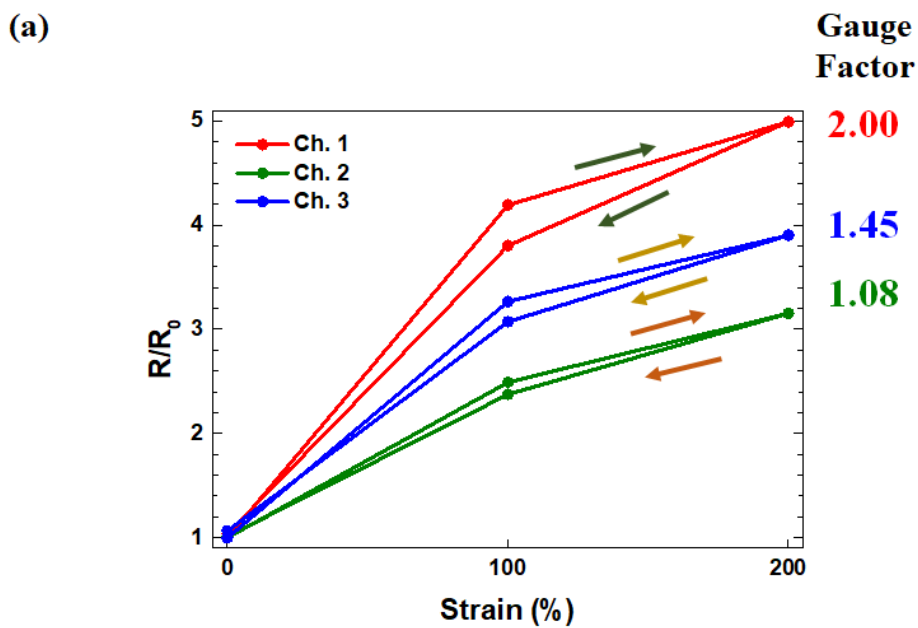


Figure 19. Volume-Resistance characteristics with the 3-channel strain sensor on a balloon-model. (a) The resistance and (b) the resistance change rate according to the volume.

Figure 19 shows the result of applying a 3-channel strain sensor to a balloon-model to measure the resistance characteristics of according to the volume. The sensor was attached to the center of the balloon with the channel 1 facing upwards. Also, this experiment was conducted in the range of 200 mL as the same one described in the section of 3.3. The graph in Figure 19(b) shows the resistance change rate for each channel. The resistance change rate at the maximum volume of 200 mL for each channel was 3.84 ± 0.10 (5 cycles average), 3.98 ± 0.01 (5 cycles average), and 4.28 ± 0.11 (5 cycles average), respectively.

However, in our strain sensors, AuCNT composites are deposited using the electrodeposition methods, so their composition is very random. Therefore, it is very difficult to control the gage factor of all channels at the same level. Therefore, we cannot measure the length of the strain sensor stretched using the resistance change rate. Accordingly, we measured gauge factor of each channel and applied it to the resistance change rate.

Figure 20(a) shows the gauge factors of each channel of the 3-channel strain sensor we used in the balloon model. The gauge factors of each channel we measured were 2.00, 1.08, and 1.45. We attempted to apply these values to the resistance change rate of each channel to determine the relative expansion.



(b)

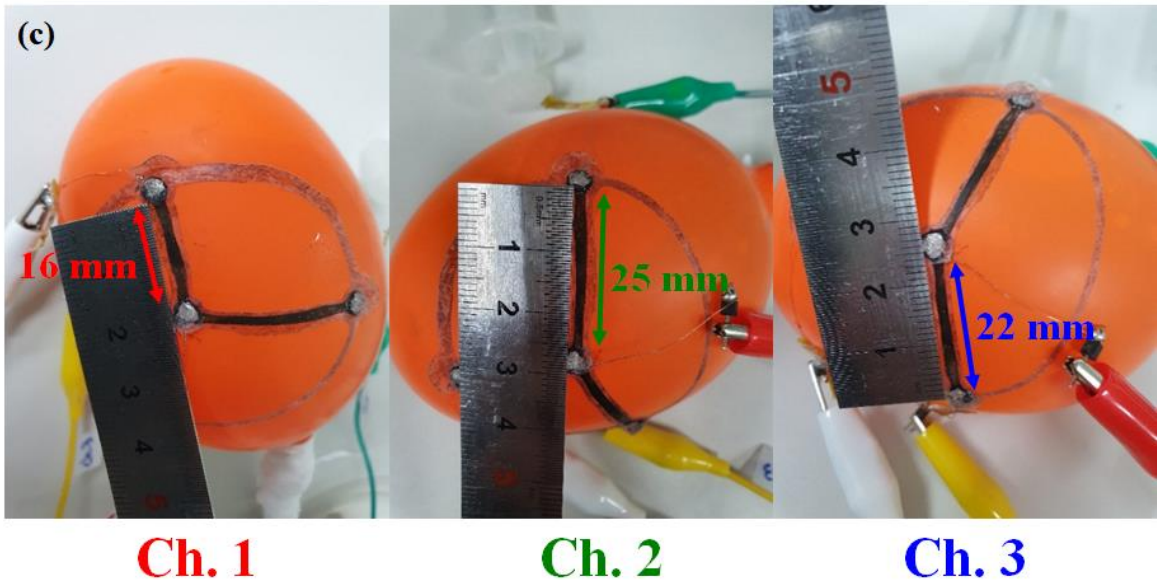
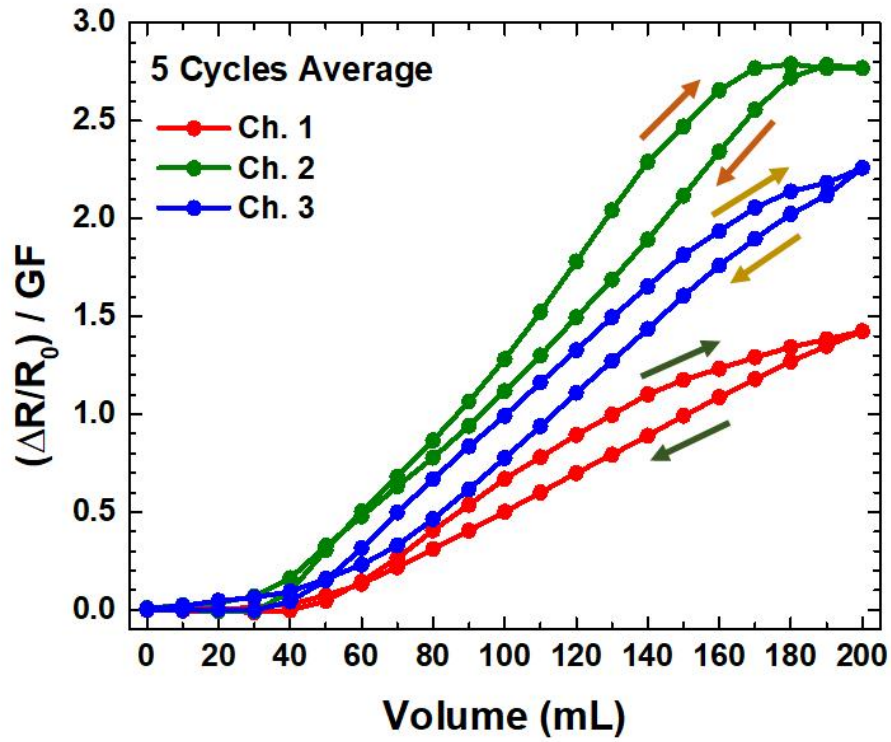


Figure 20. Expansion detecting of the balloon-model. (a) Gauge factor at 200 % strain of each channel. (b) Relative expansion of the sensor by applying each gauge factors. (c) The length of each channel at volume of 200 mL.

The graph in Figure 20(b) shows the relative expansion of each channel calculated using gauge factors, that was mentioned in the section of 2.7. Also, Figure 20(c) shows the stretched length of each channel in a 200 mL balloon. In Figure 20(a), the relative expansion values for each channel were 1.42, 2.77, and 2.26, respectively. According to Figure 20(b), the lengths of each channel at 200 mL were 16 mm (60 % strain), 25 mm (150 % strain), and 22 mm (120 % strain). Both results showed trends in channel 2 > channel 3 > channel 1. Therefore, we demonstrate that our 3-channel strain sensor can measure the relative expansion of the balloon, in each direction.

Next, we tracked the expansion direction of pig's bladder using our 3-channel strain sensor, that demonstrated to be able to measure the relative expansion direction through resistance changes. Figure 21 shows a fixed 3-channel strain sensor using surgical suture and silicone elastomer on the wall of a pig's bladder. We measured the resistance according to the volume with 3-channel strain sensor to track the relative expansion direction of the pig's bladder within 600 mL, as shown in the section of 3.4.

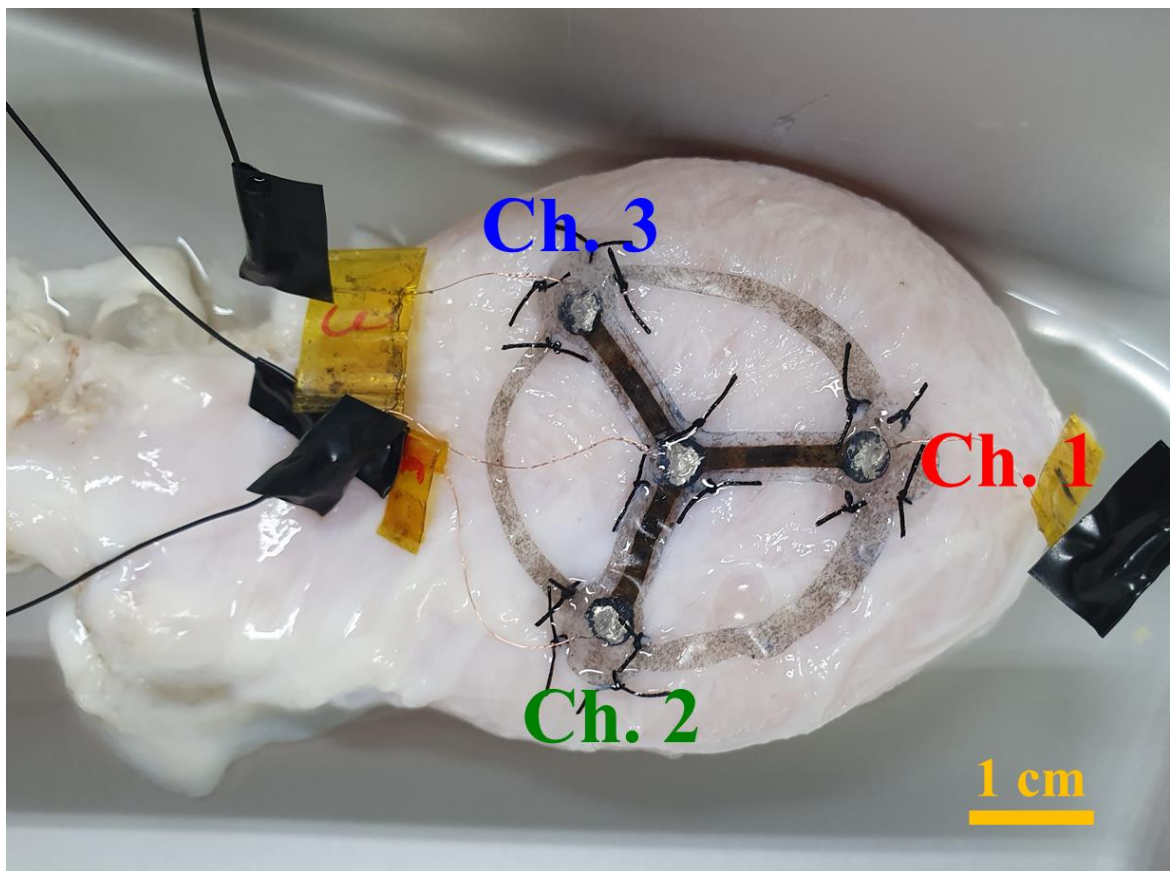
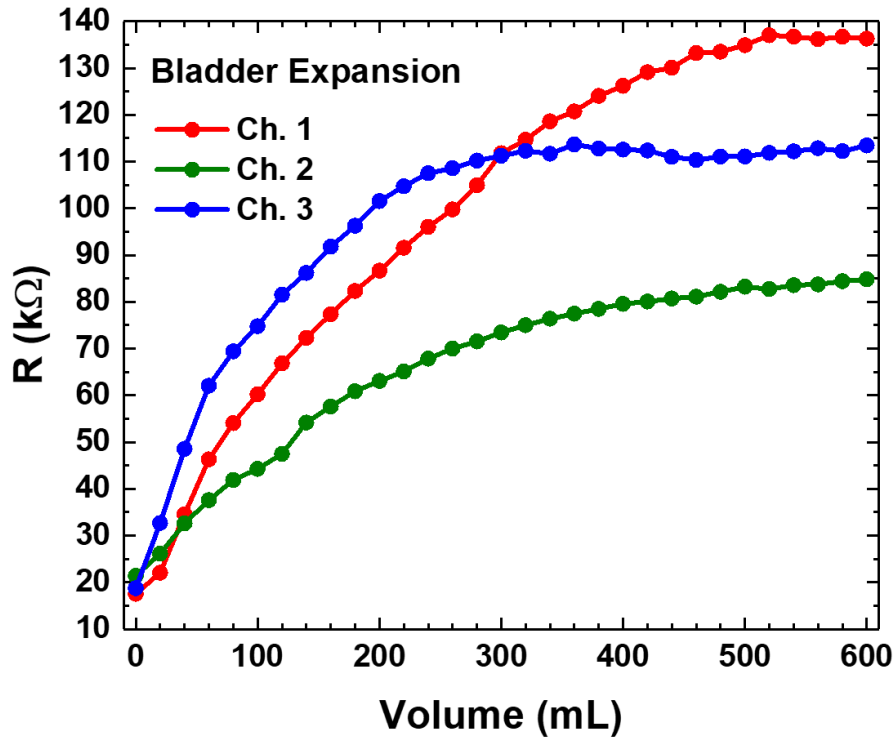


Figure 21. The 3-channel strain sensor sutured on the bladder wall.

(a)



(b)

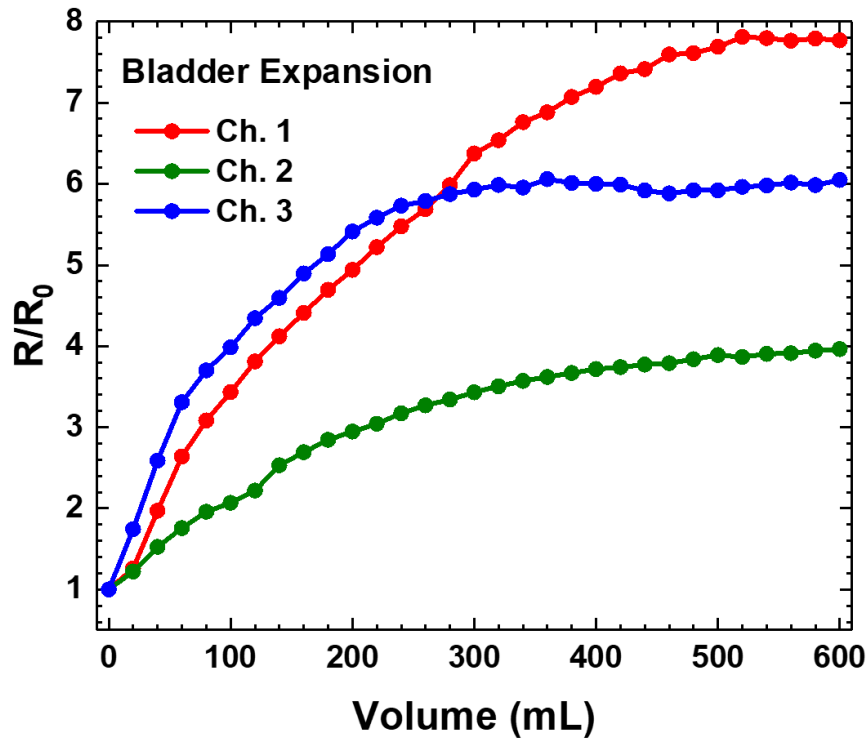
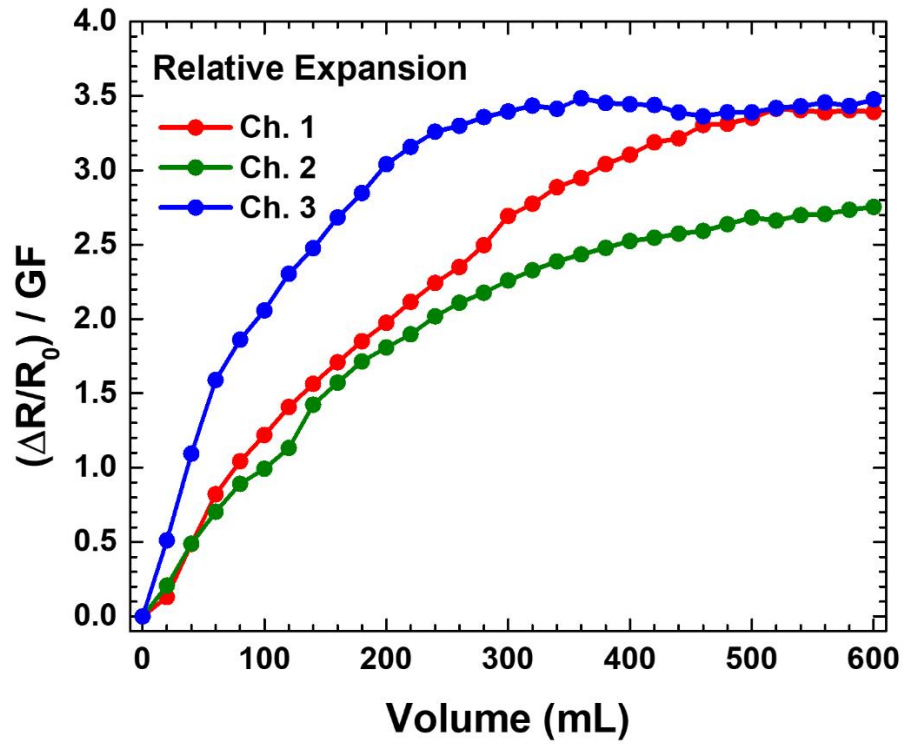


Figure 22. Volume-Resistance characteristics of 3-channel strain sensor with a pig's bladder. (a) The resistance and (b) the resistance change rate according to the volume.

(a)



(b)

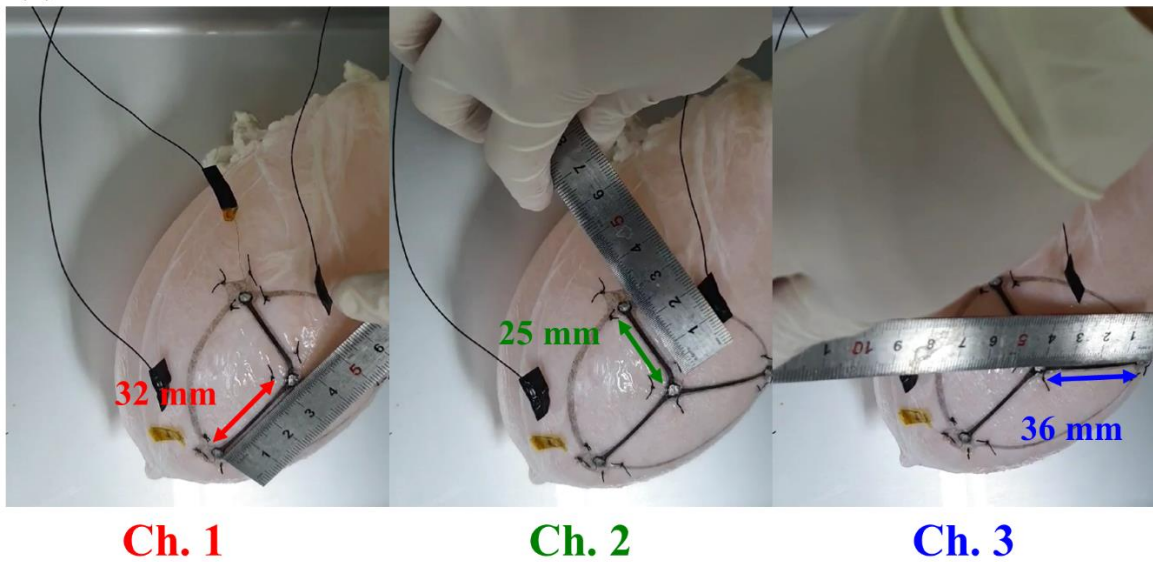


Figure 23. *Ex-vivo* test of 3-channel strain sensor for detecting of expansion directions. (a) Relative expansion of the sensor by applying each gauge factors. (b) The length of each channel at volume of 600 mL.

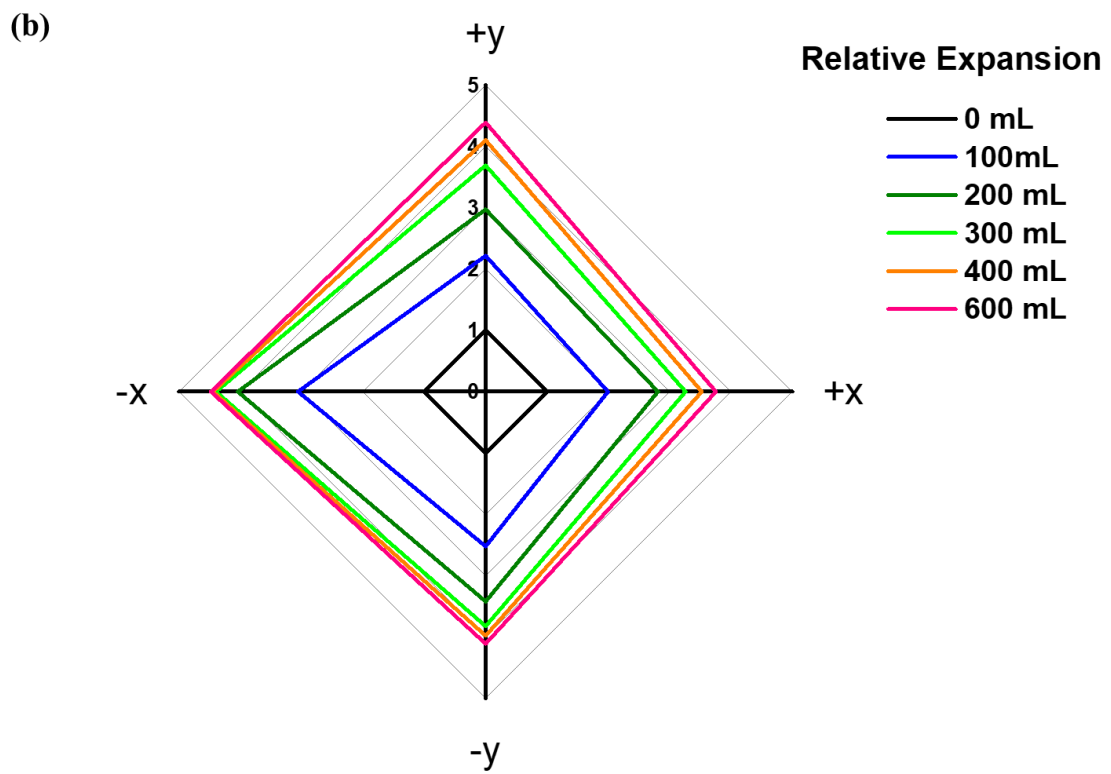
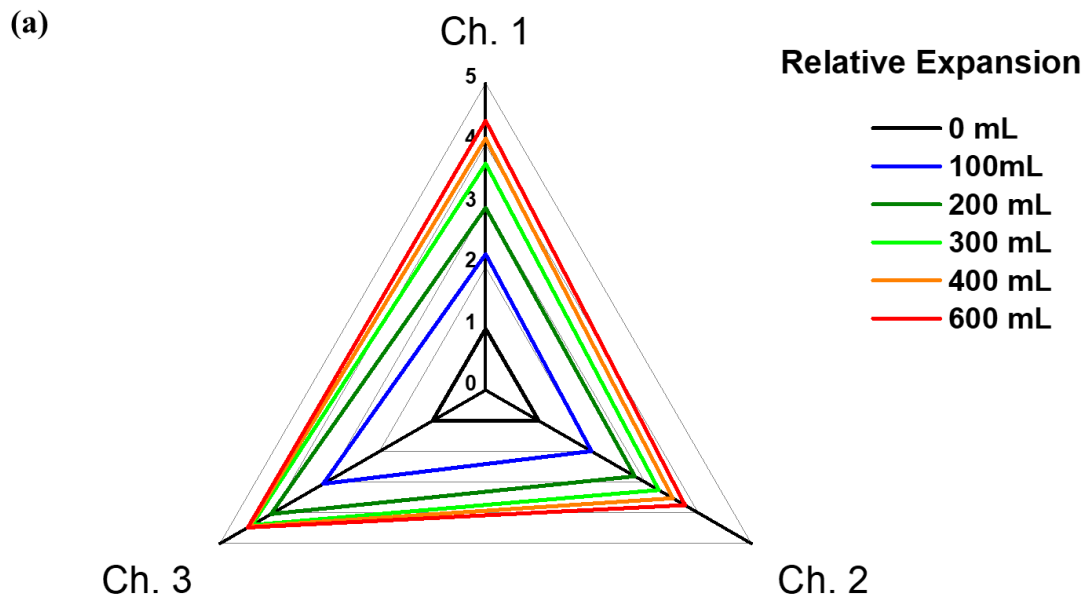


Figure 24. Bladder expansion according to the volume. (a) by each channel. (b) on the x - y coordinates.

Figure 22 shows the resistance change of each channel of the 3-channel strain sensor according to the volume of the pig's bladder. According to Figure 22(b), when the volume of the bladder was 600 mL, the resistance change rate of each channel were 7.77, 3.96, and 6.05, respectively. Figure 23 also shows the relative expansion of the bladder at a volume of 600 mL and the length of each channel. In Figure 23(a), when the volume of the bladder was 600 mL, the relative expansion values of each channel were 3.39, 2.75, and 3.48, respectively. And, as shown in Figure 23(b), the lengths of each channel were 32 mm (220 % strain), 25 mm (150 % strain), and 36 mm (260 % strain), respectively. This result also showed the same tendency as channel 3 > channel 1 > channel 2, as the result in the balloon-model.

In the result of Figure 23(a), we indirectly measured which direction the bladder wall expanded more depending on the volume of the bladder. Based on these results, we drew two graphs of Figure 24 in order to intuitively see in which direction the bladder expanded as its volume increased. Figure 24(a) is a graph drawn according to the coordinates of a 3-channel strain sensor, and Figure 24(b) is a graph converted to x - y coordinates using the formula in Figure 8(b). We also tracked the relative expansion of each channel, assumed that when the resistance is R_0 , the relative expansion is 1. As a result, it was shown that the volume of pig's bladder we used was rapidly expanding in the $-x$ direction up to 300 mL, and after that, uniformly in the $+x$ and $+y$ directions. The result demonstrated that a 3-channel strain sensor was sufficiently capable of tracking the direction of expansion according to the volume of the bladder.

Meanwhile, at the end of the section of 3.4, we discussed the effect of the pressure from the curvature of the bladder on the resistance of the strain sensor. We used the following formula to define the error values between the actual strain and the calculated strain with the resistance change rate and the gauge factor.

$$\left(1 - \frac{L/L_0}{\frac{\Delta R/R_0}{GF} + 1}\right) \times 100 \%$$

We calculated the error of the result with stick-shaped strain sensor in the section of 3.4, and the error of the result with 3-channel strain sensor using the above formula. As a result, the error of the stick-shaped strain sensor was 39.19 % and the errors of the 3-channel strain sensor were calculated as 27.02 %, 33.17 %, and 19.69 % respectively for each channel. We experimentally proved that the curvature of the bladder wall affects the evaluation of the strain sensors attached on the wall. Considering this issue, therefore, we proposed the 3-channel strain sensor and demonstrated that the shorter the length of the strain sensor, the less the effect of pressure from the curvature of the bladder on the resistance of the strain sensor.

IV. CONCLUSION

Flexible and stretchable strain sensors and its monitoring system were developed for bladder volume monitoring. Ecoflex-CNT strain sensors were developed considering the characteristics of the bladder, and the fabrication conditions were optimized. Also, AuCNT composites were additionally deposited on the CNT film to increase the sensitivity of the strain sensor. The performance test of the proposed strain sensor up to 200 % strain was conducted. The results showed that the gauge factor of the AuCNT composited strain sensor was about 5 times higher than the one with only CNT.

In addition, the measurement platform was developed with Arduino, water pumps, and flow sensors to apply the AuCNT strain sensors to a balloon-model. The resistance of the strain sensor according to the volume of the balloon-model in the range of 200 mL was measured. At the same time, the measured results were applied to the monitoring systems consisting of Arduino and LEDs, so that the amount of volume was indicated by the LEDs. The results showed that our strain sensor and monitoring system reliably tracked the volume of the balloon in the range of 200 mL.

To demonstrate the proposed sensor for practical bladder applications, the same strain sensor was applied to pig's bladders. The resistance according to the volume in the range of 600 mL was measured. The result showed that our strain sensors operated well till the maximum volume of the bladder.

Finally, a 3-channel strain sensor was developed to track the direction of expansion of the bladder. It was also applied to the balloon-model and pig's bladders. As a result, the 3-channel strain sensor tracked the relative expansion of the balloon or the bladder with resistance changes.

The overall results demonstrate that our Ecoflex-AuCNT strain sensors and the monitoring system show positive potential for monitoring the bladder volume. However, all of these experiments were conducted *ex-vivo* and in room temperature environments. Toward clinical applications, *in-vivo* experiments should be conducted. After that, we expect that the propose sensor and system may potentially provide a closed-loop platform with a neurostimulator for underactive bladder (UAB) in the future.

References

- [1] Lee, S., Wang, H., Peh, W. Y. X., He, T., Yen, S. C., Thakor, N. V., & Lee, C. "Mechano-neuro-modulation of autonomic pelvic nerve for underactive bladder: A triboelectric neurostimulator integrated with flexible neural clip interface." *Nano Energy*, 60, 2019, pp. 449-456.
- [2] Hannah, S., Brige, P., Ravichandran, A., & Ramuz, M. "Conformable, stretchable sensor to record bladder wall stretch." *ACS Omega*, 4(1), 2019, pp. 1907-1915.
- [3] Lee, S., Wang, H., Peh, W. Y. X., Thakor, N. V., Yen, S. C., & Lee, C. "Direct Stimulation of Bladder Pelvic Nerve using Battery-Free Neural Clip Interface." *2019 9th International IEEE/EMBS Conference on Neural Engineering (NER)*, San Francisco, CA, USA, 2019, pp. 706-709.
- [4] Tammela, T., & Arjamaa, O. "Comparison of long-term and short-term stretch on rat urinary bladder in vitro." *Urological Research*, 16(4), 1988, pp. 277-280.
- [5] Van Mastriegt, R. "Mechanical properties of (urinary bladder) smooth muscle." *Journal of Muscle Research & Cell Motility*, 23(1), 2002, pp. 53-57.
- [6] Pokrywczynska, M., Jundzill, A., Adamowicz, J., Kowalczyk, T., Warda, K., Rasmus, M. et al. "Is the Poly (L-Lactide-Co-Caprolactone) Nanofibrous Membrane Suitable for Urinary Bladder Regeneration?." *PLoS One*, 9(8), 2014, pp. e105295.
- [7] Yan, D., Bruns, T. M., Wu, Y., Zimmerman, L. L., Stephan, C., Cameron, A. P. et al. "Ultra-compliant carbon nanotube direct bladder device." *Advanced healthcare materials*, 8(20), 2019, pp. 1900477.
- [8] Mickle, A. D., Won, S. M., Noh, K. N., Yoon, J., Meacham, K. W., Xue, Y. et al. "A wireless closed-loop system for optogenetic peripheral neuromodulation." *Nature*, 565(7739), 2019, pp. 361-365.
- [9] Kim, M. K., Lee, S., Yoon, I., Kook, G., Jung, Y. S., Bawazir, S. S. et al. "Polypyrrole/Agarose Hydrogel-Based Bladder Volume Sensor with a Resistor Ladder Structure." *Sensors*, 18(7), 2018, pp. 2288.
- [10] Stauffer, F., Zhang, Q., Tybrandt, K., Llerena Zambrano, B., Hengsteler, J., Stoll, A. et al. "Soft electronic strain sensor with chipless wireless readout: toward real-time monitoring of bladder volume." *Advanced Materials Technologies*, 3(6), 2018, pp. 1800031.
- [11] Weydts, T., Brancato, L., Soebadi, M. A., De Ridder, D., & Puers, R. "A novel method to investigate bladder wall behavior by acceleration and pressure sensing." *Sensors and Actuators A: Physical*, 280, 2018, pp. 376-382.
- [12] Majerus, S. J., Fletter, P. C., Ferry, E. K., Zhu, H., Gustafson, K. J., & Damaser, M. S. "Suburothelial bladder contraction detection with implanted pressure sensor." *PloS one*, 12(1), 2017, pp. e0168375.

- [13] Clausen, I., Tvedt, L. G. W., Hellandsvik, A., Rognlien, D. K. W., & Glott, T. "An in vivo MEMS sensor system for percutaneous measurement of urinary bladder." *2017 39th Annual International Conference of the IEEE Engineering in Medicine and Biology Society (EMBC)*, Jeju Island, Korea, 2017, pp. 1857-1860.
- [14] Arab Hassani, F., Mogan, R. P., Gammad, G. G., Wang, H., Yen, S. C., Thakor, N. V., & Lee, C. "Toward self-control systems for neurogenic underactive bladder: a triboelectric nanogenerator sensor integrated with a bistable micro-actuator." *ACS nano*, 12(4), 2018, pp. 3487-3501.
- [15] Na Ni and Ling Zhang. *Dielectric Elastomer Sensors*, IntechOpen, London, 2017, 235 pages
- [16] Wu, S., Peng, S., & Wang, C. H. "Stretchable strain sensors based on PDMS composites with cellulose sponges containing one-and two-dimensional nanocarbons." *Sensors and Actuators A: Physical*, 279, 2018, pp. 90-100.
- [17] Kanbur, Y., & Tayfun, U. "Investigating mechanical, thermal, and flammability properties of thermoplastic polyurethane/carbon nanotube composites." *Journal of Thermoplastic Composite Materials*, 31(12), 2018, pp. 1661-1675.
- [18] Amjadi, M., Yoon, Y. J., & Park, I. "Ultra-stretchable and skin-mountable strain sensors using carbon nanotubes–Ecoflex nanocomposites." *Nanotechnology*, 26(37), 2015, pp. 375501.
- [19] Park, J., Jang, I. R., Lee, K., & Kim, H. J. "High Efficiency Crumpled Carbon Nanotube Heaters for Low Drift Hydrogen Sensing." *Sensors*, 19(18), 2019, pp. 3878.
- [20] Jo, J. W., Jung, J. W., Lee, J. U., & Jo, W. H. "Fabrication of highly conductive and transparent thin films from single-walled carbon nanotubes using a new non-ionic surfactant via spin coating." *Acs Nano*, 4(9), 2010, pp. 5382-5388.
- [21] Meyyappan, M., Delzeit, L., Cassell, A., & Hash, D. "Carbon nanotube growth by PECVD: a review." *Plasma Sources Science and Technology*, 12(2), 2003, pp. 205.
- [22] Meitl, M. A., Zhou, Y., Gaur, A., Jeon, S., Usrey, M. L., Strano, M. S., & Rogers, J. A. "Solution casting and transfer printing single-walled carbon nanotube films." *Nano Letters*, 4(9), 2004, pp. 1643-1647.
- [23] Zhou, Y., Hu, L., & Grüner, G. "A method of printing carbon nanotube thin films." *Applied physics letters*, 88(12), 2006, pp. 123109.
- [24] Kim, T., Song, H., Ha, J., Kim, S., Kim, D., Chung, S. et al. "Inkjet-printed stretchable single-walled carbon nanotube electrodes with excellent mechanical properties." *Applied Physics Letters*, 104(11), 2014, pp. 113103.
- [25] Lee, S., Yen, S. C., Sheshadri, S., Delgado-Martinez, I., Xue, N., Xiang, Z. et al. "Flexible epineurial strip electrode for recording in fine nerves." *IEEE Transactions on Biomedical Engineering*, 63(3), 2015, pp. 581-587.

요 약 문

방광의 부피 모니터링을 위한 유연하고 신축성 있는 변형 센서

본 논문은 방광의 부피를 모니터링 하기 위해 생체 적합성이 높은 재료로 만들어진 매우 유연하고 신축성 있는 변형 센서(Strain Sensor) 및 모니터링 시스템에 대해 다룬다.

방광 질환은 고령화 사회에서 새롭게 대두되고 있는 문제 중 하나로, 전세계적으로 많은 사람들이 이로 인해 고통받고 있다. 최근 방광 질환 치료를 위한 방법 중 하나로 신경 자극 기법이 주목을 받고 있다. 허나 이를 적용하기 위해서는 자극의 적절한 시점을 알 수 있도록 방광의 상태를 효과적으로 모니터링 하기 위한 방법이 필요하다. 이를 위해 방광의 상태를 모니터링 하기 위한, 체내 삽입이 가능한 비침습형 센서가 다양하게 연구되어 왔다. 하지만 이들 중 상당수는 높은 신축성이 요구되는 방광의 특성에 완전히 부합되지 않았다. 또한, 센서와 함께 모니터링을 통한 방광의 움직임을 관찰한 연구가 매우 적다.

방광은 팽창함에 따라 그 벽의 길이가 3 배까지 늘어나는 특성을 가지고 있다. 이에 따라 생체 적합성이 높고, 낮은 영률을 가지고 있으며, 충분히 신축성 있는 물질인 Ecoflex 를 사용하였다. 또한, 모니터링 시스템의 간편함을 위해 저항 변화 센서로 제작을 하였으며 이를 위해 신축성 있는 전도성 물질인 탄소 나노 튜브(CNT)의 박막을 Ecoflex 위에 형성하였다. 그리고 탄소 나노 튜브만으로 제작된 변형 센서의 낮은 민감도를 보완하기 위해 금-탄소 나노 튜브 복합체(AuCNT Composites)를 탄소 나노 튜브 박막 위에 형성하였다. 간단한 막대 모양으로 제작된 센서로 탄소나노튜브 센서와 금-탄소나노튜브 복합체 센서의 성능을, 200 % 변형에서의 저항 변화 특성을 측정하여 비교하였으며, 센서의 민감도가 약 5 배 향상되었음을 보였다. 그리고 풍선 모델과 돼지 방광에서의 부피에 따른 저항 특성을 측정하였으며, 아두이노를 사용해 만든 저항 변화 모니터링 시스템을 통해 방광 모니터링의 가능성을 보였다.

더 나아가 방광이 팽창함에 따라 보이는 방광 벽의 움직임을 추적하기 위해 3 개의 채널을 가진 센서를 디자인하였다. 앞서 성능을 평가한 금-탄소나노튜브 복합체 센서를 같은 공정을 통해 3 채널로 제작하였다. 또한, 아두이노를 사용하여 유량에 따른 센서의 저항 변화를 추적할 수 있는 시스템을 개발하였고, 이를 이용해 3 채널 센서의 성능을 측정하였다. 이로써 신경 자극 기법으로 방광 질환을 치료하기 위한, 체내 삽입 가능한 시스템의 가능성을 보이고자 한다.

핵심어: 변형 센서, 방광 질환, 모니터링 시스템. 금-탄소나노튜브, 폐회로 신경 자극